Ribosome rescue inhibitors clear *Neisseria gonorrhoeae in vivo* using a new mechanism

Zachary D. Aron[1, †], Atousa Mehrani[2, †], Eric D. Hoffer[3, †], Kristie L. Connolly[4], Matthew C. Torhan[1], John N. Alumasa[5], Pooja Srinivas[3], Mynthia Cabrera[5], Divya Hosangadi[5], Jay S. Barbor[1], Steven C. Cardinale[1], Steven M. Kwasny[1], Lucas R. Morin[1], Michelle M. Butler[1], Timothy J. Opperman[1], Terry L. Bowlin[1], Ann Jerse[4], Scott M. Stagg[2,6], Christine M. Dunham[3], Kenneth C. Keiler[5,*]

[1]Microbiotix, Inc. One Innovation Dr., Worcester, MA 01605, USA
[2]Department of Chemistry and Biochemistry, Florida State University
[3]Department of Biochemistry and Emory Antibiotic Resistance Center, Emory University School of Medicine
[4]Department of Microbiology and Immunology, Uniformed Services University, Bethesda, MD
[5]Department of Biochemistry & Molecular Biology, Penn State University
[6]Institute of Molecular Biophysics, Florida State University
*Correspondence to: kkeiler@psu.edu
[†]These authors contributed equally

PDB accession code: 6OM6; EM accession code: EMD-20121

SUPPLEMENTAL TEXT

Structure-Activity Relationships

Compound optimization studies first focused on evaluation of overall structure activity relationships (SAR), resulting in a large data set, a selection of which is shown in Table S1. Analyses focused on the 4 conceptual zones of the molecule (Figure 1A). Although only partial details on SAR data are included here, a more detailed analysis will be the topic of a future publication.

Zone 1 was tolerant of aliphatic, aromatic and heteroaromatic groups (entries 1-3, Table S1; heteroaromatics not shown), but complete replacement of the Zone 1 substituent with a hydrogen atom was not tolerated (entry 4, Table S1). It should be noted that, although incorporating aliphatic groups in Zone 1 moderately increased potency, extensive oxidative metabolism at this site limited further work in this direction (not shown).

The oxadiazole ring (Zone 2) was critical to activity, with only oxadiazoles and oxazoles displaying measurable, if widely varied, activity, despite evaluation of >20 heterocycles (representative examples include entries 1, 5-6, Table S1). This high level of specificity is consistent with hydrogen-bonding and/or dipole-directed interactions with this moiety in the binding site, as these properties vary widely among oxadiazoles (*1*).

Efforts to identify amide isosteres or alternatives in Zone 3 that avoid the observed amidolysis in KKL-35 proved challenging because variation of the amide was poorly tolerated. Of >10 isosteres examined, only analogs containing amides, ureas or *N*-alkyl amides were tolerated (entries 1, 7-9, and 12-16, Table S1). This specificity is consistent with binding interactions involving the oxygen of the Zone 2 amide and a requirement for planarity in this region of the molecule. Although replacement of the amide with a urea prevented amidolysis, simple ureas such as MBX-4346 (entry 12, Table S1) still demonstrated limited microsomal stability, consistent with aliphatic ring oxidation.

Variations in Zone 4 examined both amides and ureas. Among the amides, changes that disrupt coplanarity with the Zone 2 amide were poorly tolerated (*e.g.* aliphatics or C-2 substituents; entries 10 and 11, Table S1). Aromatic groups were well tolerated in Zone 1, with hydrophobic substituents distal to the core leading to improved potency (not shown). Among the ureas, small rings were moderately tolerated, with 6- and 7-membered rings providing improved potency relative to 5 membered rings (entries 12-14, Table S1). Hydrophilic groups, such as the ether moiety in the morpholine ring of MBX-4697 (entry 15, Table S1) had a deleterious effect on potency, although they dramatically increased microsomal stability, consistent with limiting aliphatic group oxidation. Spirocyclic and bridged bicyclic rings had a significantly deleterious

361 effect on potency, consistent with a need for a relatively flat cross-section in this region of the
362 molecule (not shown). Fused bicyclic groups were generally well tolerated, provided they did not
363 include branching on the carbon directly attached to the urea moiety; of these, fused aryl rings
364 provided excellent enhancement in both potency and metabolic stability, resulting in the
365 identification of MBX-4132 (entry 16, Table S1).

366 Throughout SAR studies, *in vitro* ADME properties such as solubility, microsomal stability and
367 cytotoxicity were monitored. Most compounds exhibited cytotoxicity profiles favorable for
368 development and moderate-to-good solubility, likely due to the hydrophilic 1,3,4-oxadiazole
369 moiety (*1*). An initial concern was metabolic stability, with the Zone 2 amide providing a particular
370 liability. Replacement of this group with a urea moiety provided a clear solution to the problem
371 (entries 12-16, Table S1). Further evaluation of MBX-4132 focused on ligand efficiency, serum
372 effects and permeability (Table S2). These studies revealed excellent drug-like properties and
373 predicted the observed oral bioavailability. It should be noted that MBX-4132 is highly serum-
374 bound, a feature that has an impact on its potency in the presence of serum (Table S2).
375

376 SUPPLEMENTAL METHODS

377 **Chemical Synthesis**

378 All commercially obtained reagents and solvents were used as received. ^{1}H and ^{13}C NMR spectra
379 were recorded on a Bruker 300 MHz instrument. Chemical shifts are given in d values referenced
380 to the internal standard tetramethylsilane (*2*). LC/MS analyses were performed on a Thermo-
381 Finnigan Surveyor LC unit connected to a Thermo LTQ Fleet MS unit. HPLC purification was
382 performed on a Gilson Unipoint instrument equipped with a 00G-4252-P0-AX C18, 10 micron,
383 150 mm or 250mm x 21.2 mm column from Phenomonex. Silica column purification was
384 performed on Isco brand Combi-flash R_f liquid chromatography system using 50□m silica
385 Luknova SuperSep columns. Melting points were taken on EZ-Melt automated melting point
386 apparatus (Stanford Research Systems, Inc.) in manual mode, and are uncorrected. Thin-layer
387 chromatography was performed on silica gel GHLF plates from Analtech (Newark, DE), and the
388 chromatograms were visualized under UV light at 254 nm. 5-(4-fluorophenyl)-1,3,4-oxadiazol-2-
389 amine, 3-phenyl-1,2,4-oxadiazol-5-amine were purchased from Enamine (Kiev, Ukraine); 5-
390 phenyl-1,2,4-oxadiazol-3-amine was purchased from Chembridge (San Diego, CA, USA); 5-
391 cyclohexyl-1,3,4-oxadiazol-2-amine, 1,3,4-oxadiazol-2-amine were purchased from Life
392 Chemicals (Niagara-on-the-Lake, ON, Canada); p-Toluenesulfonyl Chloride, 1,1'-
393 Carbonyldiimidazole were purchased from Thermo Fisher Scientific (Acros Organics) (New
394 Jersey, USA); 4-Chlorobenzoyl chloride was purchased from Thermo Fisher Scientific (Alfa

395 Aesar) (New Jersey, USA); 2-amino-5-phenyl-1,3,4-oxadiazole amine, 4-Chlorobenzoic acid,
396 Cyclohexanecarboxylic acid, 4-Chlorobenzaldehyde, Pyrrolidine, Piperidine,
397 Hexamethyleneimine, Morpholine, Methyl Iodide, Sodium Triacetoxyborohydride,
398 Diisopropylethyl amine, Triethylamine, and all solvents were purchased from Millipore-Sigma (St.
399 Louis, MO, USA); 1,2,3,4-tetrahydro-isoquinoline and 4-chlorobenzene sulfonyl chloride were
400 purchased from Combi-Blocks (San Diego, CA, USA); 4-methyl-1,2,3,6-tetrahydropyridine
401 hydrochloride was purchased from Pharmablock (Hatfield, PA, USA); HATU was purchased from
402 GenScript (Piscataway, NJ, USA).
403 *General Method A:* Heteroaryl amine (1.1eq) was dissolved in NMP (0.29 M) and triethylamine
404 (1.2 eq) stirred for 10 min at room temperature; to this solution, acid chloride (1 eq) was added
405 dropwise via pipette. The reaction mixture was allowed to continue stirring at room temperature
406 for 16-20 h. If the reaction did not reach completion, the mixture was warmed to 50°C for an
407 additional 16-20 h. Upon completion, reaction mixture was added to water, and the resulting
408 precipitate was filtered and dried. Crude precipitate purified with HPLC (5-95% MeCN/H_2O + 0.1%
409 TFA).
410 *General Method B:* Carboxylic acid (1.1 eq) and HATU/HBTU (1.2 eq) were dissolved in NMP
411 (0.28 M), to which N,N-diisopropylethylamine (1.2 eq) and heteroaryl amine (1 eq) were added.
412 The reaction was stirred at room temperature for 16-20hr. If the reaction did not reach completion,
413 the mixture was warmed to 50°C for an additional 16-20hr. Upon completion, reaction mixture
414 was added to water, and the resulting precipitate was filtered and dried. Crude precipitate purified
415 with HPLC (5-95% MeCN/H_2O + 0.1% TFA).
416 *General Method C:* To oxadiazole amine (eq) and 1,1'-Carbonyldiimidazole (1 eq) in N-methyl
417 imidazole (0.56 M) was added 3 Å () molecular sieves (1.6mm pellets: ~4 pellets/mmol). Reaction
418 was stirred at room temperature for 3-16 h. Then, the second amine (1.1 eq) was added to the
419 reaction and continued stirring at room temperature for 2-18 h. Upon completion, reaction mixture
420 was added to water, and the resulting precipitate was filtered and dried. Crude precipitate purified
421 with HPLC (5-95% MeCN/H_2O + 0.1% TFA).
422 KKL-35/MBX-3535: Prepared according to General Method A to provide material consistent with
423 prior reports (*3*). 15.0 mg (7%); mottled tan powder; ^{1}H NMR (DMSO): 12.35 (br, 1H), 8.08-8.01
424 (m, 4H), 7.65 (d, 2H), 7.47 (t, 2H); LC/MS: 318.0 (M+1); mp: >240°C (decomp.); R_f: 0.25 (50%
425 EtOAc/hexanes).
426 MBX-4083: Prepared according to General Method A. 26.0 mg (14%); off-white solid; ^{1}H NMR
427 (DMSO): 12.75 (br s, 1H), 8.07-7.99 (m, 4H), 7.67-7.58 (m, 5H); LC/MS: 300.0 (M+1); mp: 182-
428 188°C; R_f: 0.64 (50% EtOAc/hexanes).

429 MBX-3943: Prepared according to General Method A. 12.0 mg (6%); white solid; ^{1}H NMR
430 (DMSO): 11.77-11.68 (m, 1H), 8.14-7.91 (m, 4H), 7.76-7.53 (m, 5H); LC/MS: 300.2 (M+1); mp:
431 >102°C (slow); R_f: 0.65 (50% EtOAc/hexanes).
432 MBX-3910: Prepared according to General Method A to provide material consistent with prior
433 reports (*4*). 30.0 mg (16%); white solid; ^{1}H NMR (DMSO): 12.26 (br, 1H), 8.08-7.96 (m, 4H), 7.67-
434 7.62 (m, 5H); LC/MS: 300.2 (M+1); mp: 250-259°C; R_f: 0.34 (50% EtOAc/hexanes).
435 MBX-4370**:** Prepared according to General Method A to provide material consistent with prior
436 reports (*3*). 26.0 mg (28%); White solid; ^{1}H NMR (DMSO): 11.95 (bs, 1H), 8.02-8.00 (m, 2H), 7.64-
437 7.61 (m, 2H), 2.94 (m, 1H), 2.02-1.98 (m, 2H), 1.77-1.41 (m, 8H); LC/MS: 306.2 (M+1); mp: 204-
438 206°C; R_f: 0.72 (5% MeOH/DCM).
439 MBX-4367: Prepared according to General Method A. 17.0 mg (13%); white solid; ^{1}H NMR
440 (DMSO): 12.12 (bs, 1H), 9.10 (s, 1H), 8.06-7.98 (m, 2H), 7.65-7.59 (m, 2H); LC/MS: 224.0 (M+1);
441 mp: 212-214°C; R_f: 0.32 (5% MeOH/DCM).
442 MBX-C4227: Material was purchased and tested as received from Life Chemicals, Inc.
443 MBX-3709: Prepared according to General Method A. 150 mg (97%); light brown solid; ^{1}H NMR
444 (DMSO): 11.66 (s, 1H), 7.99-7.95 (m, 2H), 7.47-7.41 (m, 2H), 1.87-1.66 (m, 6H), 1.41-1.22 (m,
445 6H); LC/MS: 290.0 (M+1); mp: >205°C (slow); R_f: 0.73 (3.75:46.25:50 MeOH/EtOAc/DCM).
446 MBX-3776: Prepared in a manner to that previously described (*5*), by dissolving (E/Z)-N-(4-
447 chlorobenzylidene)-5-(4-fluorophenyl)-1,3,4-oxadiazol-2-amine (0.331mmol, 1.0 eq), and
448 $NaHB(OAc)_3$ (0.430 mmol, 1.3 eq) in dichloromethane (1 ml), stirred at room temperature for 18
449 h. Adsorbed material onto Celite and isolated product from column chromatography eluted with
450 linear gradient of 0-50% EtOAc in Hexanes. 27.0 mg (27%); White solid; ^{1}H NMR (DMSO): 8.39
451 (t, 1H), 7.87-7.82 (m, 2H), 7.41-7.34 (m, 6H), 4.43 (d, 2H); LC/MS: 304.1 (M+1); mp: 165-167°C;
452 R_f: 0.42 (50% EtOAc/hexanes).
453 MBX-4076: Prepared by dissolving 4-chloro-N-(5-(4-fluorophenyl)-1,3,4-oxadiazol-2-
454 yl)benzamide (MBX-3535, 0.220 mmol, 1.0 eq) in DMF (2 ml), to which K_2CO_3 (0.264 mmol, 1.1
455 eq) was added and the mixture was stirred at room temperature for 2 h. Then methyl iodide (0.220
456 mmol, 1.0 eq) was added and continued to stir at room temperature for an additional 65 h. The
457 reaction was diluted with water (~30 ml), solid precipitate was filtered and dried under high
458 vacuum. Product was purified by HPLC (20-100% MeCN/H_2O + 0.1% TFA) and freeze dried to
459 solid. 13.0 mg (18%); White solid; ^{1}H NMR ($CDCl_3$): 8.21 (d, 2H), 8.01-7.97 (m, 2H), 7.40 (d, 2H),
460 7.22 (t, 2H), 3.74 (s, 3H); LC/MS: 332.2 (M+1); mp: >148°C (slow); R_f: 0.66 (50%
461 EtOAc/hexanes).

462 MBX-4063**:** Prepared according to modified General Method A; used solvent mixture of
463 Pyridine/Dichloromethane (1/1 mixture) instead of NMP and triethylamine. 33.0 mg (18%); white
464 solid; ^{1}H NMR ($CDCl_3$): 7.96-7.86 (m, 4H), 7.34-7.16 (m, 4H + CHCl3), 2.42 (s, 3H); LC/MS: 334.1
465 (M+1); mp: 218-221°C; R_f: 0.14 (50% EtOAc/hexanes).
466 MBX-4346**:** Prepared according to General Method C. 15.0 mg (20%); light yellow solid; ^{1}H NMR
467 ($CDCl_3$): 7.98-7.95 (m, 2H), 7.20-7.14 (m, 2H), 3.57 (m, 4H), 1.96 (m, 4H); LC/MS: 277.1 (M+1);
468 mp: 197-199°C; R_f: 0.94 (10% MeOH/DCM).
469 MBX-4699: Prepared according to General Method C. 13.0 mg (9%); white solid; ^{1}H NMR ($CDCl_3$):
470 7.97-7.92 (m, 2H), 7.21-7.15 (m, 2H), 3.65 (m, 4H), 1.62 (m, 6H); LC/MS: 291.5 (M+1); mp: 200-
471 203°C; R_f: 0.64 (10% MeOH/DCM).
472 MBX-4700: Prepared according to General Method C. 15.0 mg (33%); white solid; ^{1}H NMR ($CDCl_3$
473 + MeOD): 7.92-7.88 (m, 2H), 7.13-7.07 (m, 2H), 3.48 (m, 4H), 1.69 (m, 4H), 1.52-1.50 (m, 4H);
474 LC/MS: 305.7 (M+1); mp: 191-194°C; R_f: 0.63 (10% MeOH/DCM).
475 MBX-4697: Prepared according to General Method C. 8.9 mg (15%); white solid; ^{1}H NMR ($CDCl_3$
476 + MeOD): 7.93-7.89 (m, 2H), 7.18-7.12 (m, 2H), 3.66 (m, 8H); LC/MS: 293.9 (M+1); mp: 211-
477 216°C; R_f: 0.55 (10% MeOH/DCM).
478 MBX-4366: Prepared according to General Method C. 19.0 mg (23%); white solid; ^{1}H NMR
479 ($CDCl_3$): 7.98-7.93 (m, 2H), 7.21-7.16 (t, 2H), 5.41 (m, 1H), 4.11 (m, 2H), 3.78 (m, 2H), 2.11 (m,
480 2H), 1.73 (s, 3H); LC/MS: 303.0 (M+1); mp: 180-181°C; R_f: 0.74 (5% MeOH/DCM).
481 MBX-4132: Prepared according to General Method C; dried precipitate solids were triturated in
482 MeOH (~50mL) yielded pure product. 375 mg (40%); white solid; ^{1}H NMR (DMSO): 7.98-7.94 (m,
483 2H), 7.46-7.40 (m, 2H), 7.19 (s, 4H), 4.69 (s, 2H), 3.75 (t, 2H), 2.85 (t, 2H); LC/MS: 339.1 (M+1);
484 mp: >190°C (slow); R_f: 0.51 (50% EtOAc/hexanes).
485
486 **Bacterial Strains and Growth Conditions**
487 Bacterial strains, plasmids, and synthetic sequences are shown in Table S9. *E. coli* strains
488 expressing L27 were constructed by transducing a *tolC::cat* allele into IW312 strains using a P1
489 *vir* phage. These strains were grown in LB medium containing 1 mM IPTG. To quantify the *in vitro*
490 antibacterial activity of acylaminooxadiazole analogs against various bacterial strains, the
491 minimum inhibitory concentration (MIC) was measured using microbroth dilution assays as
492 described in the CLSI guidelines (M7-A7) (*6*), except that liquid G77L medium (*7*) was used for
493 *Neisseria gonorrhoeae* MIC assays. Each assay comprised three technical replicates, and each
494 assay was repeated at least once. The reported MIC is the geometric mean of at least 5 technical

495 replicates. H041(STM^R) is a streptomycin-resistant derivative of the multi-drug resistant (MDR),
496 ceftriaxone-resistant strain H041 (Ohnishi) and was cultured as previously described (*8–10*).
497
498 **Time-kill assays**
499 The time kill assay was performed essentially as described (*11*) with the following modifications
500 for *N. gonorrhoeae*. The bacterial inoculum for the assays was prepared by suspending colonies
501 of *N. gonorrhoeae* ATCC 49226 grown on a chocolate agar plate for >24 h (37 °C with 5% CO_2)
502 in G77L medium. The cell suspension was adjusted to an OD_{600} of 0.1 and was diluted 1:10 in
503 G77L media (final cell density ~1 × 10^7 cells/ml) containing various concentrations of MBX-4132.
504 The resulting cultures were incubated at 37 °C (5% CO_2), and viability was monitored over 24 h
505 by removing samples at various time points, making serial 10-fold dilutions in G77L, and spotting
506 5 µl of each dilution onto the surface of a chocolate agar plate in triplicate. Colonies were counted
507 after the plates were incubated at 37 °C (5% CO_2) for 18-18 h, colony forming units (cfu) per ml
508 were calculated, and the average and standard deviation for the three replicates was determined.
509 The lower limit of detection of this assay was determined to be 100-200 cfu/ml. This experiment
510 was repeated three times, and the results of a representative experiment are shown.
511
512 ***In vitro trans*-translation and translation assays**
513 The *in vitro trans*-translation assay is designed to produce the first 157 amino acids of nano-
514 luciferase from a non-stop mRNA (nanoluc-ns) and add the C-terminal peptide
515 AAVSGWRLFKKIS via a mutant version of *E. coli* tmRNA (tmRNA-nl) to reconstitute an active
516 nano-luciferase (*12*). In this assay, the tagged nano-luciferase gene has >30,000-fold increase in
517 activity over the peptide made in the absence of tmRNA-nl.
518 S12 lysates were made according to the procedure of Kim, et al., (*13*). Briefly, a culture of *E.*
519 *coli* BL21 (DE3) cells containing a pET28 plasmid carrying the *E. coli* T7 polymerase gene was
520 grown at 37 °C to an OD_{600} = 0.8, induced with 1 mM IPTG and grown for an additional 3 h. Cells
521 were harvested by centrifugation at 20,000 *g* for 10 min at 4°C and the pellet was resuspended
522 in buffer A (20 mM Tris-acetate (pH 8.2), 14 mM $Mg(OAc)_2$, 60 mM potassium glutamate, 1 mM
523 DTT). Cells were lysed by sonication, the lysate was clarified by centrifugation at 12,000 *g* for 10
524 min, and the supernatant was stored at -80 °C.
525 *E. coli* SmpB was purified as previously described (*14*). tmRNA-nl, a variant of *E. coli* tmRNA
526 encoding the final 11 residues of nano-luciferase, was transcribed from the tmRNA-nl synthetic
527 DNA sequence in vitro, purified, and folded as previously described for wild-type *E. coli* tmRNA
528 (*14*). The nanoluc-stop template DNA was prepared as previously described (*14*) by PCR

529 amplification from pMC1 using T7 universal and nanoluc-stop primers. The nanoluc-ns was
530 prepared in a similar manner using pMC1 with T7 universal and nanoluc-ns primers.
531 For *in vitro trans*-translation, tmRNA-nl and SmpB were premixed and stored on ice. S12
532 lysate (2 μl), freshly made polymix buffer (2 μl) (*15*) (final reaction concentrations 5 mM Hepes
533 pH 7.6, 5 mM NH_4Cl, 0.5 mM $CaCl_2$, 1.5 mm $MgCl_2$, 1 mM DTT, 8 mm putrescene, 2 mm ATP, 2
534 mM GTP, 1 mM CTP, 1 mM UTP, 0.3 mM each amino acid, 3 mg/ml *E. coli* tRNAs), nanoluc-ns
535 template (0.5 μl; 60 ng) and 2 μl water were mixed and incubated at 37 °C for 5 min. This solution
536 was dispensed to tubes containing 0.5 μl of different concentrations of an inhibitor prepared in
537 75% acetonitrile, 25% water, and incubated at 37 °C for 5 min. The tmRNA-nl/SmpB mixture (0.5
538 μl each, 2 μM final) was added to each tube and the samples were incubated at 37 °C for 1.5 h.
539 NanoLuc substrate (Promega) was prepared according to the manufacturer's instructions, one
540 volume of this substrate solution was added to each sample tube, and the reactions transferred
541 to a white 96-well plate. Luminescence readings were obtained using the SpectraMax i3
542 microplate reader. Data analysis was performed using GraphPad Prism 8.
543
544 **Frequency of resistance**
545 First, MIC values were determined for MBX-4132 using the reference agar dilution method (*6*,
546 *16*). *N. gonorrhoeae* strain 49226 (ATCC) was suspended to the equivalent of a 5 McFarland
547 standard in G77L broth and then diluted to generate the final inoculum (1.5 x 10^5). The bacterial
548 cell suspension was then transferred to wells in a stainless-steel replicator block which was used
549 to inoculate the test plates. After the inoculum had dried, all plates were incubated at 35°C in 5%
550 CO_2. The MIC was read post-incubation per CLSI guidelines (*6*, *16*). To determine the frequency
551 of resistance, stock solutions of MBX-4132 were prepared at 100X the final test concentrations of
552 4× and 8× the predetermined MIC value. A 0.5 mL aliquot of the 100X stock was mixed with 49.5
553 mL of molten GC Medium agar/1% IsoVitaleX to produce an agar/drug mixture that was either 4-
554 or 8-fold the MIC and dispensed into sterile 150 x 15 mm plates (VWR) at a volume of 50 mL per
555 plate. A dense cell suspension equivalent to 5 McFarland was prepared using bacterial growth
556 from 48 h chocolate agar plates of *N. gonorrhoeae* (ATCC 49226). The viable count of each
557 suspension was determined by plating serial ten-fold dilutions onto GC Medium agar/1%
558 IsoVitaleX in duplicate. A 0.25 ml aliquot of inoculum was spread onto the surface of duplicate
559 150 x 15 mm test plates. After allowing the inoculum to dry on the surface of the plate, the plates
560 were inverted and incubated at 35ºC (with 5% CO_2) for 48 h. Colony counts were determined
561 manually and the spontaneous mutation frequency was calculated using the following equation:
562 Average number of colonies from selection plates/Total number of cells inoculated

563 If there were no colonies on the antibiotic selection plates, the spontaneous mutation frequency
564 was calculated as 1/inoculum to indicate that the spontaneous mutation frequency was less than
565 the limit of detection (one cfu).
566
567 **Mammalian cell cytotoxicity (CC_{50})**
568 The half maximal cytotoxic concentration (CC_{50}) of each compound against HeLa cells (ATCC
569 CCL-2) was measured as previously described (*17*). Each assay comprised three technical
570 replicates, and each assay was repeated at least once. The mean values for each biological
571 replicate were averaged, and the CC_{50} was determined using a 4-parameter nonlinear curve fitting
572 algorithm (GraphPad Prism). The average of the CC_{50}s from two biological replicates was
573 calculated and reported.
574
575 **Murine liver microsome stability**
576 To examine potential for first-pass metabolism of analogs in the liver, the stability of analogs in
577 the presence of mouse liver microsome preparations (Eurofins Discovery for human, dog and rat;
578 Xenotech for mouse) was measured using the method of Kuhnz, et al. (*18*) for murine studies and
579 Oback for the dog, human and rat studies. (*19*). The amount of parent compound remaining after
580 incubation with microsomes in the presence of NADPH over a 30 min time range was measured
581 using a reverse-phase liquid chromatography/mass spectroscopy method that was customized
582 for each compound. Half-lives were calculated using linear regression analysis of several time
583 points.
584
585 **Caco-2 permeability**
586 To evaluate the potential for oral bioavailability, the ability of prioritized compounds to permeate
587 a monolayer of Caco-2 intestinal epithelial cells was determined as described (*20*). Caco-2
588 permeability values (P_{app}) >1 × 10^{-6} cm/sec are predictive of oral bioavailability. The observation
589 that $P_{app\ A\rightarrow B} > P_{app\ B\rightarrow A}$ indicates that efflux from the basolateral compartment does not occur.
590
591 **Serum Protein Binding**
592 Serum protein (fetal bovine) binding was determined using an equilibrium dialysis method as
593 described (*21*). The amount of compound in each chamber (buffer and serum) was measured
594 using methods for reverse-phase liquid chromatography/mass spectroscopy methods that were
595 customized for each compound.
596

597 **Aqueous solubility**

598 The maximum aqueous solubility of each compound was determined using a nephelometric
599 method as described (*22*). Each assay comprised three technical replicates, and each assay was
600 repeated at least once. The reported solubility is the average of at least 5 technical replicates.

601

602 **Cell-based non-stop luciferase reporter assay**

603 To verify that MBX-4132 retains activity as an inhibitor of trans-translation, we measured its dose-
604 dependent activity against the non-stop luciferase reporter assay strain E. coli SB75 ΔtolC::kan
605 (pluc-trpAt) essentially as described (*14*), with modifications. Briefly, serial 1.5-fold dilutions of
606 MBX-4132 in DMSO were transferred to 96-well assay plates (Costar 3195), followed by the
607 addition of 50 µl of an overnight culture of SB75 ΔtolC::kan (pluc-trpAt) that had been diluted to a
608 final OD_{600} of 0.4 with LB media supplemented with 100 µg ampicillin/ml and 1 mM IPTG. The
609 final concentrations of MBX-4132 ranged from 0.05 – 1.5 µM, and the final concentration of DMSO
610 was 2%. The assay plates were incubated at room temperature for 2 h, and 50 µl of BrightGlo
611 (Promega) bioluminescence reagent was added to each well. After 10 min incubation,
612 bioluminescence intensity was measured using an Envision multi-label plate reader (Perkin
613 Elmer). Each assay comprised three technical replicates, and the experiment was repeated three
614 times. The fold induction for each MBX-4132 treated sample as compared to the DMSO-only
615 sample was calculated for each technical replicate, and the average and standard deviation of
616 the three technical was calculated. The IC_{50} was determined using a 4-parameter nonlinear curve
617 fitting algorithm (GraphPad Prism).

618

619 **CYP450 Inhibition, Receptor Panel Profiling, and Cardiac Ion Channel Profiling**

620 Several *in vitro* selectivity assays were performed at Eurofins Discovery Services using
621 established methods and controls that behaved as expected (Tables S5 & S6). For CYP450
622 inhibition assays, activity of MBX-4132 was tested at 5 concentrations from 30 nM to 100 µM; no
623 inhibitory activity >50% was observed at any concentration. For receptor panel profiling, MBX-
624 4132 was evaluated at 10 µM and activity of >50% (agonist or antagonist) was scored as active.

625

626 **Ames Assay**

627 The Ames assay was performed at SRI Biosciences, following the standard protocols established
628 there (*23–25*). In brief, samples were evaluated for their ability to induce genetic damage using
629 the plate incorporation method with *Salmonella typhimurium* strains TA98 and TA100 with and
630 without a metabolic activation mixture containing 10% Aroclar-1254-induced rat-liver microsomes

631 (S9). MBX-4132 was tested from a 5 mg/mL DMSO stock solution (the solubility limit), which
632 provided plate concentrations up to 500 µg/plate, with serial dilutions accessing doses as low as
633 5 µg/plate. MBX-4132 precipitated at the two highest dose levels (500 and 100 µg/plate), but at
634 50 µg/plate, no precipitation was observed. Precipitation did no interfere with colony counts or
635 analysis. Test articles were considered mutagenic when the mean number of revertant colonies
636 increased in a dose-dependent manner. Some cytotoxicity was observed, but sufficient colonies
637 were formed to allow analysis. As shown in Table S6, MBX-4132 exhibited no significant deviation
638 in revertant colonies from the DMSO control at any concentration tested. Data for 2-nitrofluorene
639 and sodium azide (positive controls) and DMSO (negative control) were included for reference.
640

641 **Mitochondrial Toxicity Assays (performed at Eurofins Cerep Panlabs)**

642 *Multiplexed cytotoxicity assay*

643 Human primary hepatocytes were grown on collagen I coated optical plates, cultured in
644 hepatocytes culture media in a humidified 5% CO_2 atmosphere at 37 ˚C. Cells were incubated in
645 the presence of MBX-4132 at 10 concentrations starting a 100 µM and serially diluted 3.16-fold
646 for 24 h at 37 °C, incubated for 30 min with multiplexed fluorescent dyes (Hoescht, 6-carboxy-
647 2',7'-dichlorodihydrofluorescein diazetat, and TMRE) and imaged to allow visualization of nuclei,
648 reactive oxygen species generation, and mitochondrial oxidation. A >3.5-fold induction of ROS
649 was considered consistent with formation of ROS and a >2-fold change in TMRE signal indicated
650 an increase or decrease in mitochondrial membrane potential (*26*).

651 *Mitochondrial toxicity assay*

652 HepG2 cells were seeded and cultured in media containing either glucose or galactose overnight.
653 Test compounds were added at 8 concentrations (3-fold serial dilution from 100 µM to 30 nM) and
654 incubated with the cells for 24 h. Cell viability was measured by the alamarBlue method. The data
655 in Table S7 are inconsistent with MBX-4132 disrupting mitochondrial metabolic processes (*27*).
656

657 **Pharmacokinetic analyses in mice**

658 *For PO suspension dosing* (Performed at Neosome LLC):

659 Female CD-1 mice were fasted for 2 h prior, and 4 h after dosing. MBX-4132 was administered
660 male BalB/C mice at 10 mL/kg via oral gavage with a 1.0, 2.5 or 10.0 mg/ml suspension in vehicle
661 A (5% DMSO, 5% Cremophor EL®, 0.45% hydroxypropylmethylcellulose, 0.45% alginic acid,
662 22.5% hydroxy-betacyclodextrin). At 0.25, 0.5, 1, 2, 4, 8 and 24 h post dose, 3 mice from each
663 group were euthanized by CO_2 inhalation, blood was collected by cardiac puncture into K_2EDTA

664 collection tubes, and protein was precipitated and analysed by LC/MS-MS for plasma
665 concentrations of MBX-4132. Data were analysed using WinNonLin.
666 *For IV and SC dosing* (performed at Charles River Labs)*:*
667 MBX-4132 was administered at 6 ml/kg via direct tail vein puncture (IV, slow push), oral gavage
668 (PO) or subcutaneously to the intrascapular region (SC) in a 2 mg/ml 10% DMSO/80% PEG-
669 400/10% water formulation. For oral dosing, mice were fasted for 2 h prior and four hours post
670 dosing. At 0.083, 0.5, 1, 4, 8 and 24 h post dose, blood was collected from 3 mice/group by tail
671 vein or facial bleed into K_2EDTA collection tubes, and protein was precipitated and analysed by
672 LC/MS-MS for plasma concentrations of MBX-4132. Sampling was performed serially, with each
673 mouse contributing sample at all time points. Data were analysed using WinNonLin.
674
675 **Murine tolerability studies**
676 (All testing was performed at Neosome LLC)
677 *Single dose tolerability studies:*
678 Female CD-1 mice were fasted for 2 h prior, and 4 h after dosing. MBX-4132 was administered
679 at 10 ml/kg via oral gavage with a 0.0 (vehicle control), 1.0, 2.5 or 10.0 mg/ml suspension in
680 vehicle A. Mice were observed at 0.083, 0.25, 0.5, 1, 2, 5, 8 and 24 h post dosing, and any
681 abnormal observations (behaviour, agility, coat condition and appearance, color of urine, quality
682 of feces, etc.) were noted. No abnormal observations of any dosing group were made during the
683 24 h course of this study.
684 *Multidose tolerability studies:*
685 In preparation for this study, an abbreviated version of the above murine PK study using the same
686 formulation examined fasted mice vs. fed mice was performed, with plasma samples taken at 1
687 and 4 h post dosing and analyses as described in the PK section. No significant variation in
688 exposure was observed at either timepoint.
689 Female CD-1 mice were given free access to food and water. MBX-4132 was administered to
690 groups of 3 mice for 7 d either QD (with compound) or BID (two groups, one vehicle only and one
691 with compounds) at 10 ml/kg via oral gavage with a 1.0 mg/ml suspension in A. Mice were
692 observed twice daily for 10 d (3 d post final dose), additionally, mice were weighed daily. Any
693 abnormal observations (behaviour, agility, weight, coat condition and appearance, color of urine,
694 quality of feces, etc.) were noted. No abnormal observations of any dosing group were made
695 during the 24 h course of this study. One mouse in the vehicle only group did exhibit a slight
696 weight loss but had recovered weight by the end of the study.
697

698 ***In vivo* efficacy testing in the gonorrhea mouse model**

699 Groups of female BALB/cAnNCr mice (Charles River Laboratories) (6-7 weeks old) were treated
700 with 17β-estradiol and antibiotics (streptomycin and trimethoprim) to increase susceptibility to
701 long-term *N. gonorrhoeae* infection as described (*8*). Mice were inoculated vaginally with *N.*
702 *gonorrhoeae* strain H041 (10^4 cfu/mouse) two days after estradiol pellet implantation and vaginal
703 swabs were cultured for two days post-bacterial inoculation to confirm infection. On the afternoon
704 of the second culture day (day 0), mice were given MBX-4132, GEN or the vehicle (n= 20-21
705 mice/group). Doses of MBX-4132 were prepared fresh in vehicle at the time of treatment and
706 administered as a single oral dose (dose volume 10 ml/kg). The positive control GEN (48 mg/kg)
707 was prepared and administered intraperitoneally as 5 daily doses as previously described (*8*).
708 Vaginal swabs were collected on 8 consecutive days following treatment and quantitatively
709 cultured for *N. gonorrhoeae* to assess efficacy. The data are expressed as CFU/ml of vaginal
710 swab suspension. Clearance was shown by Kaplan-Meier curves with log-rank (Mantel-Cox)
711 statistical analysis. The average cfu/ml over time was compared by 2-way ANOVA with Bonferroni
712 post-hoc analysis. Statistics were performed in GraphPad Prism Software. At the study endpoint
713 (10 days post-inoculation), mice were euthanized using compressed CO_2 gas in a CO_2 gas
714 chamber in the Laboratory Animal Medicine Facility. All animal experiments were conducted at
715 the Uniformed Services University of the Health Sciences, a facility fully accredited by the
716 Association for the Assessment and Accreditation of Laboratory Animal Care, under a protocol
717 that was approved by the university's Institutional Animal Care and Use Committee.

718

719 **Purification of stalled ribosome complexes**

720 To construct pET28-H10arfArnc, a DNA cassette encoding 10 histidine residues, the M2 epitope,
721 3 glycine residues, and 20 arbitrary codons followed by 71 base pairs from the 3' end of the *E.*
722 *coli arfA* gene was synthesized and assembled into pET28 that had been digested with NcoI and
723 HindIII (*28*). The sequence from *arfA* contains the RNase III cleavage site (*29*, *30*). Translation of
724 the cleaved mRNA produces a 59 amino acid peptide with 10 histidines at the N terminus.
725 *E. coli* 70S ribosomes were purified as described previously (*31*). *E. coli* BL21(DE3) pET28-
726 H10arfArnc cells were grown to an A_{600} of ~0.5 in Luria broth (LB) medium at 37 °C and induced
727 with 1 μM IPTG and 1 μM KKL-2098 (synthesized as previously described (*32*)) and continued to
728 grow for an additional hour at 37 °C then cooled on ice for 20 min. All centrifugation steps were
729 performed at 4 °C. Cells were pelleted by centrifugation and washed with buffer 1 (10 mM HEPES-
730 KOH, pH 7.6, 10 mM $MgCl_2$, 1 M NH_4Cl, 6 mM β-mercaptoethanol (β-Me)) twice and then
731 resuspended in buffer 2 (10 mM HEPES-KOH, pH 7.6, 10 mM $MgCl_2$, 100 mM NH_4Cl, 6 mM β-

732 Me). The cells were crosslinked under ultraviolet light (254 nm) for 10 min, then lysed using an
733 EmulsiFlex-C5 high-pressure homogenizer (Avestin). Cell debris was removed by centrifuging at
734 13,000 × *g* for 15 min. The lysate was further centrifuged at 27,000 × *g* for 30 min to obtain the
735 S30 fraction. Ribosomes were pelleted by centrifuging at 42,000 × *g* for 17 h. The pellets were
736 resuspended in buffer 2 and bound to a 1 mL IMAC gravity column, washed with 10 column
737 volumes of Buffer 2 and eluted with Buffer 2 supplemented with 500 μM imidazole. Ribosomes
738 were further purified over a 10–40% sucrose gradient in buffer 2 at 70,000 × *g* for 12 h. 70S
739 ribosomes were separated from polysomes and subunits using a Brandel gradient fractionator.
740 The 70S fractions were pooled, pelleted, resuspended in buffer 2, and stored at −80 °C.
741
742 **Cryo-Electron Microscopy**
743 UltrAuFoil® grids (Quantifoil, R1.2/1.3) were glow-discharged for 20 s with a Solarus 950 (Gatan).
744 3 μl of 70S complexes at 100 nM were placed on grids at 8 °C in 100% humidity and blotted for
745 3.5 s using a Vitrobot Mark IV (FEI).
746 Two independent datasets of 2,394 micrographs total (1863 and 531 micrographs,
747 respectively) were collected on a Titan Krios (FEI) microscope operated at 300 kV with a C2
748 aperture diameter of 70 μm. Movie frames were recorded at an accumulated dose of 58 $e^-/A^{\circ 2}$ at
749 a magnification of 59,000X (corresponding to a pixel value of 1.191 Å) with a DE-64 direct electron
750 detector in counting mode (*33*) using Leginon (*34*) for automatic data acquisition. Images were
751 recorded with a total exposure time of 19.3 s, and intermediate frames were recorded every 0.2
752 s giving a total of 78 frames per image. Two independent datasets of 70S ribosomes specimens
753 were collected with an overall of 2,394 micrographs (1863 and 531 micrographs from the first and
754 the second datasets, respectively). Defocus values ranged from -1.3 to -3 μm. All the pre-
755 processing steps were performed in the Appion (*35*).
756
757 **Image processing**
758 **Pre-processing**
759 All processing steps were carried out using Appion (*35*). All frames of each micrograph were
760 aligned using MotionCor2 (*36*). Contrast transfer function (CTF) parameters were estimated on
761 all motion-corrected micrographs using CTFFIND4 (*37*) and GCTF (*36*) and the best estimate
762 chosen using resolution evaluation in Appion (*38*). 197 micrographs were excluded after manual
763 visualization of their corresponding power spectra displayed ice contamination, exposure to the
764 shifted beam, or low-resolution Thon ring profiles. An initial set of ~2000 particles were picked
765 using DoG (Difference of Gaussian) Picker (*39*). A rotational average was generated from these

picks, and this was used as a template for template-based picking using FindEM (*40*). A total of 474,382 particles (373,845 and 100,537 particles from the first and the second dataset, respectively) were picked. Particles were extracted with a box size of 384x384 pixels in Appion.

Extracted particles from the two datasets were processed independently and combined after the last round of 3D reconstruction, and subjected to further 3D classifications and refinements in RELION-3 (*41*) (Figure S2). Processing steps were initially performed on a 4X-binned dataset.

Initial 3D refinement occurred against a 60 Å low-pass filtered empty *E. coli* 70S ribosome from a previous dataset. 3D classification without alignment was used to discard free 50S subunits. The resulting 70S classes were combined and refined using an initial angular sampling of 7.5° and local angular sampling of 1.8° to improve angular assignment. Following refinement, another round of 3D classification without alignment was performed, with low resolution particles and particles containing E-site tRNA discarded. Two classes with an unrotated 70S were combined and subjected to refinement, followed by focused classification with a P-site mask. The P-site mask was generated from a 70S ribosome with P-site tRNA (PDB ID 4V4I) (*42*), with a 5-voxel expansion and a 7-voxel soft edge. This resulted in a class of 70S particles with P-site tRNA. These particles were unbinned, refined, then underwent focused classification with an A site mask, created as stated, using a model of the 70S ribosome with A-site tRNA (PDB ID 4V5D) (*43*). Classes with P-site tRNA but no A-site tRNA were refined and post-processed.

Post-processing and beam-tilt correction

The resultant map was post-processed in RELION using a solvent mask generated from the final reconstruction low-pass filtered to 40 Å with a 7-pixel extension and 10-pixel soft edge. Beam-tilt estimation and correction was performed (without per-particle refinement of CTF parameters) using CTF refinement followed by 3D reconstruction. These steps were repeated iteratively until the highest resolution was achieved, and the final map post-processed with a solvent mask. Resolution estimations were calculated from Fourier shell correlations (FSC) at 0.143 between the two independently refined half-maps. Maps were sharpened in PHENIX (*44*). The graphs of directional 3D FSC and global resolution of the maps were plotted using 3DFSC Processing Server (*45*). Local resolution was estimated using blocres in Bsoft (*46*).

797 SUPPLEMENTAL TABLES

798 Table S1: Properties of acylaminooxadiazoles (subset of SAR analogs).

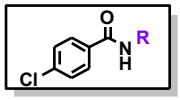

#	CMPD#	R	*Luc* IC_{50}[a]	Δ*tolC E. coli* MIC[b]	*Ng* MIC[b]	CC_{50}[c]	Sol[d]	MLMS[e]
1	KKL-35/ MBX-3535	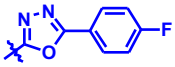	0.23	0.49	0.12	>100	25	<5
2	MBX-3910	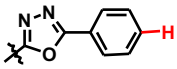	0.14	1.9	0.30	40	13	5
3	MBX-4370	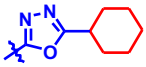	0.13	0.48	0.12	17	50	<5
4	MBX-4367	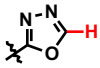	>25	22.3	11.2	>100	>200	8
5	MBX-4083	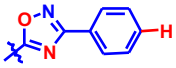	1.4	2.7	4.8	>100	6.3	<5
6	MBX-3943	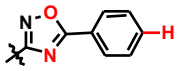	>25	>30	15.0	>100	13	<5

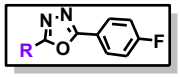

#	CMPD#	R	*Luc* IC_{50}[a]	Δ*tolC E. coli* MIC[b]	*Ng* MIC[b]	CC_{50}[c]	Sol[d]	MLMS[e]
7	MBX-3776	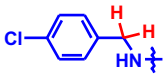	>25	>30	>30	>100	25	5
8	MBX-4076	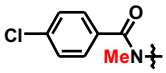	1.05	4.6	2.7	95	<3.1	
9	MBX-4063	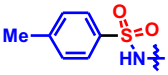	>25	>33	>33	>100	100	53
10	MBX-3709	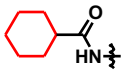	12.5	28.9	4.6	>100	25	<5
11	MBX-C4227	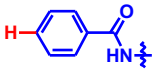	1.0	0.88	1.1	>100	50	
Urea Variants								
12	MBX-4346	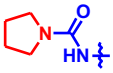	14.3	27.6	4.4	>100	>200	25
13	MBX-4699	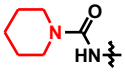	2.1	7.3	0.58	>100	50	12
14	MBX-4700	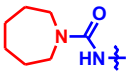	1.8	4.8	0.61	>100	25	10
15	MBX-4697	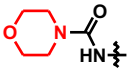	9.2	29.2	4.7	>100	100	>120
16	MBX-4132	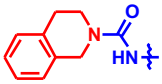	0.19	2.7	0.18	45	100	>120

[a] Half Maximal activity in Δ*tolC E. coli* luciferase assay (μM) [b] MIC vs *Neisseria gonorrhoeae* (49226) or E. coli KLE701 in μg/mL. [c] Against HeLa cells (μM). [d] Solubility in water (μM; nephlometry). [e] Murine liver microsome stability, $t_{1/2}$ in min at 37 °C in the presence of NADPH.

799

800

801 Table S2: In Vitro ADME Properties

	Microsomal Stability ($t_{1/2}$; min)				serum		Serum Binding (% bound)				Caco-2 ($P_{app;}$ x 10^{-6} cms^{-1})	
	Murine	Rat	Dog	Hum.	Shift[a]	Stab[b]	Murine	Rat	Dog	Human	A→B	B→A
MBX-4132	>120	>120	>120	>120	12	>99.8	98.0	93.0	99.0	99.0	11.1	7.3
[a]Ratio of MIC +/- 10% fetal bovine serum added. [b]% remaining after 1 h incubation at 37 ˚C.												

802

803

804

805 Table S3: Anti-gonococcal spectrum

Strain	Resistance/Description	MIC (µg/ml)	
		KKL-35	MBX-4132
ATCC 49226	type strain	0.12	0.13
ATCC 700719	SPT	0.25	0.21
ATCC 700825	STR	0.06	0.04
BAA-1846	TET	0.06	0.04
HO41	PEN, TET, CFM, CRO, LVX	0.25	0.17
CDC-0165	CIP, PEN, TET	n.d.	0.68
CDC-0166	CIP, PEN, TET	n.d.	0.17
CDC-0167		n.d.	0.13
CDC-0169	CIP, PEN, TET	n.d.	0.17
CDC-0170	CIP, PEN, TET	n.d.	0.17
CDC-0171	CIP, PEN, TET	n.d.	0.17
CDC-0172	CIP, PEN, TET	n.d.	0.17
CDC-0173	CIP, PEN, TET	n.d.	0.17
CDC-0174	CIP, PEN, TET	n.d.	0.17
CDC-0175	CIP, PEN, TET	n.d.	0.08
CDC-0176		n.d.	0.34
CDC-0177	CIP, PEN, TET	n.d.	0.17
CDC-0178	TET	n.d.	0.34
CDC-0179	CIP, PEN, TET	n.d.	0.08
CDC-0180		n.d.	0.17
CDC-0181	CIP, PEN, TET	n.d.	0.17
CDC-0182	TET	n.d.	0.17
CDC-0183	CIP, PEN, TET	n.d.	0.34
CDC-0184	CIP, PEN, TET	n.d.	0.17
CDC-0185	CIP, PEN, TET	n.d.	0.27
CDC-0186	CIP, PEN, TET	n.d.	0.17
CDC-0187	CIP, PEN, TET	n.d.	0.34
CDC-0188	CIP, PEN	n.d.	0.17
CDC-0189	CIP, PEN, TET	n.d.	0.13
CDC-0190	CIP, PEN, TET	n.d.	0.17
WHO F		n.d.	0.06
WHO G	PEN, TET	n.d.	0.13
WHO K	CIP, PEN, TET	n.d.	0.26
WHO L	CIP,PEN, TET	n.d.	0.26

WHO M	CIP,PEN,TET	n.d.	0.13
WHO N	CIP, PEN, TET	n.d.	0.26
WHO O	PEN, TET	n.d.	0.13
WHO P	PEN, TET	n.d.	0.33
WHO U	PEN, TET	n.d.	0.13
WHO V	AZM, CIP, PEN, TET	n.d.	0.26
WHO W	CIP, PEN, TET	n.d.	0.13
WHO X	CIP, PEN, TET	n.d.	0.21
WHO Y	CIP, PEN, TET	n.d.	0.21
WHO Z	CIP, PEN, TET	n.d.	0.26
MMX ATCC 49226		0.25	0.27
MMX 6744		0.13	0.27
MMX 6746	CIP	0.13	0.14
MMX 6752	TET	0.25	0.27
MMX 6753		0.06	0.14
MMX 6757		0.06	0.07
MMX 6758		0.13	0.27
MMX 6762		0.13	0.27
MMX 6767		0.06	0.14
MMX 6771	TET	0.06	0.14
MMX 6793	CIP	0.06	0.14
MMX 6797	CIP, TET	0.06	0.14
MMX 6803	CIP	0.13	0.27
MMX 6812	CIP	0.13	0.27
MMX 6818	CIP	0.13	0.27
MMX 6819	CIP	0.13	0.14
MMX 6879		0.06	0.14
MMX 6921	CIP	0.25	0.53
MMX 6922	CIP	0.25	0.53
MMX 6983	CIP	0.25	0.53
MMX 6989		0.13	0.14
MMX 6990	CIP	0.06	0.14
MMX 6992		0.13	0.14
MMX 6996		0.13	0.27
MMX 6998	CIP	0.25	0.53
MMX 7002	CIP	0.13	0.27
MMX 7005		0.03	0.03
MIC_{90} (n)		**0.25 (32)**	**0.53 (71)**
MIC Range (n)		**0.03-0.25 (32)**	**0.03-0.68 (71)**

SPT, spectinomycin; STR, streptomycin; TET, tetracycline; PEN, penicillin G; CFM, cefixime; CRO, ceftriazone; CIP, ciprofloxacin; LVX, levofloxacin; AZM, azithromycin; MMX, Micromyx, LLC strain (these MIC assays were performed, using the broth dilution method, by Micromyx, LLC.)

806

807 **Table S4.** Antibacterial spectrum

				MIC (μg/ml)	
Category	Organism	Strain	Resistance/Description	KKL-35	MBX-4132
Gram-negative	*Escherichia coli*	KLE700		≥32	≥35
	Escherichia coli	KLE701	KLE700 *ΔtolC::tet*	0.5	2.7
	Klebsiella pneumoniae	ATCC 13883		n.d.	≥35
	Acinetobacter baumannii	ATCC 19606		>32	≥35
	Pseudomonas aeruginosa	ATCC 27853		>32	≥35
	Moraxella catarrhalis	8716		n.d.	0.04
	Legionella pneumophila	ATCC 33153		n.d.	8.7
	Haemophilus influenzae	ATCC 35056		n.d.	17.5
Gram-positive	*Staphylococcus aureus*	BAA-1717	MRSA	n.d.	1.21
	Staphylococcus aureus	MRSA-1234547263	MRSA	1	3.2
	Staphylococcus aureus	MRSA-1094	MRSA	1	3.2
	Staphylococcus aureus	ATCC 35556		1	4.2
	Staphylococcus aureus	NRS-77		1	3.2
	Staphylococcus aureus	MSSA		1	4.2
	Staphylococcus aureus	N315, NRS-70	MRSA	1.5	6.3
	Staphylococcus aureus	ATCC 25923		1.5	6.3
	Staphylococcus aureus	THC1516	MRSA	0.9	1
	Streptococcus pneumoniae	ATCC 49619		n.d.	34.9
	Mycoplasma pneumoniae	ATCC 15531		n.d.	34.9

808

809 **Table S5.** Eurofins Discovery Services *In Vitro* Safety Panel, Cyp inhibition assays and Cardiac
810 Ion Channel interaction results for MBX-4132.

Catalog ref[A]	Receptor Profiling	Species	Conc	% inhibition
104010	Cholinesterase, Acetyl, ACES	hum	10 µM	6
116030	Cycloogenase COX-1	hum	10 µM	8
118030	Cycloogenase COX-2	hum	10 µM	10
140010	Monoamine Oxidase MAO-A	hum	10 µM	-108
152300	Phosphodiesterase PDE3A	hum	10 µM	-6
154420	Phosphodiesterase PDE4D2	hum	10 µM	3
176020	Protein Tyrosine Kinase, LCK	hum	10 µM	29
200610	Adenosine A_{2A}	hum	10 µM	42
203110	Adrenergic α_{1A}	hum	10 µM	6
203630	Adrenergic α_{2A}	hum	10 µM	35
204010	Adrenergic β_1	hum	10 µM	-8
204110	Adrenergic β_2	hum	10 µM	35
206000	Androgen (testosterone)	hum	10 µM	-2
214600	Calcium Channel L-Type, Dihydropyridine	rat	10 µM	11
217050	Cannabinoid CB_1	hum	10 µM	-4
217100	Cannabinoid CB_2	hum	10 µM	-4
218030	Cholecystokinin CKK_1 (CCK_A)	hum	10 µM	66
219500	Dopamine D_1	hum	10 µM	26
219700	Dopamine D_{2s}	hum	10 µM	21
224010	Endothelin ET_A	hum	10 µM	-15
226600	$GABA_A$, Flunitrazepam, Central	rat	10 µM	3
232030	Glucocorticoid	hum	10 µM	-2
232810	Glutamate, NMDA, Agonism	rat	10 µM	8
239610	Histamine H_1	hum	10 µM	11
239710	Histamine H_2	hum	10 µM	-7
252610	Muscarinic M_1	hum	10 µM	-7
252710	Muscarinic M_2	hum	10 µM	7
252810	Muscarinic M_3	hum	10 µM	5
299031	Nicotinic Acetylcholine α4β2, Cytisine	hum	10 µM	-5
260130	Opiate $Delta_1$ (OP1, DOP)	hum	10 µM	5
260210	Opiate Kappa (OP2, KOP)	hum	10 µM	13
260410	Opiate Mu (OP3, MOP)	hum	10 µM	17

265510	Potassium Channel [K_A]	rat	10 µM	-2
265910	Potassium Channel hERG, [^{3}H Dofetilide	hum	10 µM	27
271110	Serotonin (5-hydroxytryptamine) 5-HT_{1A}	hum	10 µM	30
271230	Serotonin (5-hydroxytryptamine) 5-HT_{1B}	hum	10 µM	21
271650	Serotonin (5-hydroxytryptamine) 5-HT_{2A}	hum	10 µM	18
271700	Serotonin (5-hydroxytryptamine) 5-HT_{2B}	hum	10 µM	44
271910	Serotonin (5-hydroxytryptamine) 5-HT_3	hum	10 µM	4
279510	Sodium Channel, Site 2	rat	10 µM	21
220320	Transporter, Dopamine (DAT)	hum	10 µM	3
204410	Transporter, Norepinephrine (NET)	hum	10 µM	6
274030	Transporter, Serotonin (5-Hyroxytryptamine) (SERT)	hum	10 µM	-10
287530	Vasopressin V_{1A}	hum	10 µM	-4

Catalog ref[A]	Cyp Inhibition Assays	Species	pIC_{50}
4876	CYP1A inhibition (Phenacetin substrate)	hum	NC[B]
4877	CYP2B6 inhibition (Bupropion substrate)	hum	>100 µM
4879	CYP2C8 inhibition (Amodiaquine substrate)	hum	>100 µM
4878	CYP2C9 inhibition (Diclofenac substrate)	hum	NC[B]
4874	CYP2C19 inhibition (Omeprazole substrate)	hum	>100 µM
4875	CYP2D6 inhibition (Dextromethorphan substrate)	hum	>100 µM
4873	CYP3A inhibition (Midazolam substrate)	hum	NC[B]
4872	CYP3A inhibition (Testosterone substrate)	hum	>100 µM

Catalog ref[A]	Cardiac Ion Channel Panel	Mode	Est. IC_{50} (µM)
CYL8004QP2DR	Nav1.5	Antagonist	>30
CYL8038QP2DR	hERG	Antagonist	>30
CYL8007QP2DR	KCNQ1/mink	Antagonist	>30
CYL8069QP2DR	Kv4.3/ChIP2	Antagonist	>30 (Peak&End)
CYL8032QP2DR	Kir2.1	Antagonist	>30 (Peak&End)

CYL8051QP2DR	**Cav1.2**	**Antagonist**	**>30**
CYL7004QP1DR	**Nav1.5 late current**	**Agonist**	**>30**
CYL7004QP2DR	**Nav1.5 late current**	**Antagonist**	**>30**

[A]Assays were performed using established protocols by Eurofins Discovery Services; catalog references provided. [B]No activity observed at any tested concentration.

813 **Table S6.** Evaluation of MBX-4132 in the *Salmonella*/Microsome Plate Incorporation Assay
814 (AMES Screen) performed by SRI Biosciences, a division of SRI International.

Strain	Test Compound/Condition	Dose (µg/plate)	Mean Revertants/plate
TA98	DMSO	N/A	23.7 ± 6.7
TA100	DMSO	N/A	127.34.5 ± 4.5
TA98	DMSO+S9	N/A	28.75.9 ± 5.9
TA100	DMSO+S9	N/A	129.0 ± 4.4
TA98	2-Nitrofluorene	5	1331.3 ± 171.6
TA100	Sodium Azide	5	2029.0 ± 49.6
TA98	2-Aminoanthracene + S9	2	1206.7 ± 169.1
TA100	2-Aminoanthracene + S9	2	1438.7 ± 55.8
TA98	MBX-4132	1	21.5 ± 2.1
TA98	MBX-4132	5	17.0 ± 1.4
TA98	MBX-4132	10	15.0 ± 1.4
TA98	MBX-4132	50	20.0 ± 2.8
TA98	MBX-4132	100	20.0 ± 2.8
TA98	MBX-4132	500	17.5 ± 2.1
TA100	MBX-4132	1	112.5 ± 6.4
TA100	MBX-4132	5	99.0 ± 1.4
TA100	MBX-4132	10	97.0 ± 4.2
TA100	MBX-4132	50	73.0 ± 8.5
TA100	MBX-4132	100	54.0 ± 1.4
TA100	MBX-4132	500	35.5 ± 3.5
TA98	MBX-4132 + S9	1	23.5 ± 2.1
TA98	MBX-4132 + S9	5	22.0 ± 0.0
TA98	MBX-4132 + S9	10	21.0 ± 2.8
TA98	MBX-4132 + S9	50	18.5 ± 0.7
TA98	MBX-4132 + S9	100	17.5 ± 3.5
TA98	MBX-4132 + S9	500	20.0 ± 2.8
TA100	MBX-4132 + S9	1	107.5 ± 4.9
TA100	MBX-4132 + S9	5	125.5 ± 7.8
TA100	MBX-4132 + S9	10	102.0 ± 15.6
TA100	MBX-4132 + S9	50	71.0 ± 4.2
TA100	MBX-4132 + S9	100	43.0 ± 4.2
TA100	MBX-4132 + S9	500	19.5 ± 0.7

815

816

817

818 **Table S7.** Results from mitchondrial toxicity studies examining the effect of MBX-4132 on
819 reactive oxygen species (ROS), mitochondrial membrane potential (MMP) and differential
820 cytotoxicity against HepG2 cells grown on glucose or galactose.

Compound	Conc. (μM)	Attached live cells (%)	ROS (fold induction)	MMP inhibition (fold induction)
MBX-4132	3.18E-03	105.6 ± 7.5	3.1 ± 4.1	1.0 ± 0.1
MBX-4132	1.01E-02	109.5 ± 8.4	1.4 ± 0.4	1.0 ± 0.1
MBX-4132	3.18E-02	97.5 ± 12.2	0.9 ± 0.5	0.9 ± 0.2
MBX-4132	1.00E-01	96.7 ± 6.9	1.4 ± 1.1	1.2 ± 0.3
MBX-4132	3.17E-01	114.0 ± 14.4	1.2 ± 0.5	0.9 ± 0.1
MBX-4132	1.00E+00	106.3 ± 3.3	1.2 ± 0.4	0.9 ± 0.1
MBX-4132	3.17E+00	99.6 ± 6.1	1.1 ± 0.3	1.0 ± 0.2
MBX-4132	1.00E+01	97.7 ± 9.4	1.9 ± 1.0	1.1 ± 0.1
MBX-4132	3.16E+01	89.5 ± 3.6	1.3 ± 0.6	1.1 ± 0.1
MBX-4132	1.00E+02	69.6 ± 12.3	9.2 ± 3.6	0.8 ± 0.1
Compound	Conc. (μM)	Cell type	Medium	% viability
MBX-4132	3.00E-06	HepG2	Glucose	109.6 ± 0.2
MBX-4132	1.00E-05	HepG2	Glucose	107.8 ± 2.1
MBX-4132	3.00E-05	HepG2	Glucose	106.5 ± 3.3
MBX-4132	1.00E-04	HepG2	Glucose	85.6 ± 1.8
MBX-4132	3.00E-06	HepG2	Glucose	94.1 ± 9.3
MBX-4132	1.00E-05	HepG2	Glucose	95.4 ± 0.7
MBX-4132	3.00E-05	HepG2	Glucose	96.8 ± 0.4
MBX-4132	1.00E-04	HepG2	Glucose	64.0 ± 10.3

821

822

Table S8. Data collection, model building and refinement.

Data collection	**70S-P-tRNA-KKL-2098**
Voltage (keV)	300
Magnification	59,000
Electron dose ($e^-/Å^2$)	58
Pixel size (Å/pix)	1
Detector	DE64 counting mode
Defocus range (μm)	1.5-3.5
Micrographs	2,197
Total Particles	474,382
Reconstruction	
Particles included	28,121
$FSC_{0.5}$	3.8
$FSC_{0.143}$	3.1
Model Refinement	
CCmap_model	0.88
Model quality	
RMSD	
Bond lengths (Å) / Bond angles (°)	0.007/0.897
Ramachandran plot statistics	
Most favored (%)	94.7
Allowed	4.22
Outliers (%)	1.12
Rotamer outliers (%)	0.3
Cß outliers	0.0
Clashscore	6.66

857 **Table S9.** Bacterial strains, plasmids, and synthetic sequences.

strain name	description	source
E. coli BL21 (DE3) pET28-H10arfArnc	Strain for expressing non-stop ribosomes	this work
IW312	*E. coli* LG90 Δ*rpmA*	(*47*)
IW312 pL27	contains plasmid for inducible expression of wild-type L27	(*47*)
IW312 pL27 –3	contains plasmid for inducible expression of L27 –3	(*47*)
IW312 pL27 –6	contains plasmid for inducible expression of L27 –6	(*47*)
IW312 Δ*tolC* pL27	IW312 pL27 with *tolC* deleted	this work
IW312 Δ*tolC* pL27 –3	IW312 pL27 –3 with *tolC* deleted	this work
IW312 Δ*tolC* pL27 –6	IW312 pL27 –6 with *tolC* deleted	this work
N. gonorrhoeae H041	Clinical multiple-antibiotic resistant isolate	(*10*)
N. gonorrhoeae	ATCC 49226	ATCC
N. gonorrhoeae	ATCC 700719	ATCC
N. gonorrhoeae	ATCC 700825	ATCC
N. gonorrhoeae	BAA-1846	ATCC
N. gonorrhoeae	CDC-0165	CDC-ARBank
N. gonorrhoeae	CDC-0166	CDC-ARBank
N. gonorrhoeae	CDC-0167	CDC-ARBank
N. gonorrhoeae	CDC-0169	CDC-ARBank
N. gonorrhoeae	CDC-0170	CDC-ARBank
N. gonorrhoeae	CDC-0171	CDC-ARBank
N. gonorrhoeae	CDC-0172	CDC-ARBank
N. gonorrhoeae	CDC-0173	CDC-ARBank
N. gonorrhoeae	CDC-0174	CDC-ARBank
N. gonorrhoeae	CDC-0175	CDC-ARBank
N. gonorrhoeae	CDC-0176	CDC-ARBank
N. gonorrhoeae	CDC-0177	CDC-ARBank
N. gonorrhoeae	CDC-0178	CDC-ARBank
N. gonorrhoeae	CDC-0179	CDC-ARBank
N. gonorrhoeae	CDC-0180	CDC-ARBank
N. gonorrhoeae	CDC-0181	CDC-ARBank
N. gonorrhoeae	CDC-0182	CDC-ARBank
N. gonorrhoeae	CDC-0183	CDC-ARBank
N. gonorrhoeae	CDC-0184	CDC-ARBank
N. gonorrhoeae	CDC-0185	CDC-ARBank
N. gonorrhoeae	CDC-0186	CDC-ARBank
N. gonorrhoeae	CDC-0187	CDC-ARBank
N. gonorrhoeae	CDC-0188	CDC-ARBank
N. gonorrhoeae	CDC-0189	CDC-ARBank
N. gonorrhoeae	CDC-0190	CDC-ARBank
N. gonorrhoeae	WHO F	CDC-ARBank
N. gonorrhoeae	WHO G	CDC-ARBank
N. gonorrhoeae	WHO K	CDC-ARBank

N. gonorrhoeae	WHO L	CDC-ARBank
N. gonorrhoeae	WHO M	CDC-ARBank
N. gonorrhoeae	WHO N	CDC-ARBank
N. gonorrhoeae	WHO O	CDC-ARBank
N. gonorrhoeae	WHO P	CDC-ARBank
N. gonorrhoeae	WHO U	CDC-ARBank
N. gonorrhoeae	WHO V	CDC-ARBank
N. gonorrhoeae	WHO W	CDC-ARBank
N. gonorrhoeae	WHO X	CDC-ARBank
N. gonorrhoeae	WHO Y	CDC-ARBank
N. gonorrhoeae	WHO Z	CDC-ARBank
N. gonorrhoeae	MMX 6744	Micromyx, LLC
N. gonorrhoeae	MMX 6746	Micromyx, LLC
N. gonorrhoeae	MMX 6752	Micromyx, LLC
N. gonorrhoeae	MMX 6753	Micromyx, LLC
N. gonorrhoeae	MMX 6757	Micromyx, LLC
N. gonorrhoeae	MMX 6758	Micromyx, LLC
N. gonorrhoeae	MMX 6762	Micromyx, LLC
N. gonorrhoeae	MMX 6767	Micromyx, LLC
N. gonorrhoeae	MMX 6771	Micromyx, LLC
N. gonorrhoeae	MMX 6793	Micromyx, LLC
N. gonorrhoeae	MMX 6797	Micromyx, LLC
N. gonorrhoeae	MMX 6803	Micromyx, LLC
N. gonorrhoeae	MMX 6812	Micromyx, LLC
N. gonorrhoeae	MMX 6818	Micromyx, LLC
N. gonorrhoeae	MMX 6819	Micromyx, LLC
N. gonorrhoeae	MMX 6879	Micromyx, LLC
N. gonorrhoeae	MMX 6921	Micromyx, LLC
N. gonorrhoeae	MMX 6922	Micromyx, LLC
N. gonorrhoeae	MMX 6983	Micromyx, LLC
N. gonorrhoeae	MMX 6989	Micromyx, LLC
N. gonorrhoeae	MMX 6990	Micromyx, LLC
N. gonorrhoeae	MMX 6992	Micromyx, LLC
N. gonorrhoeae	MMX 6996	Micromyx, LLC
N. gonorrhoeae	MMX 6998	Micromyx, LLC
N. gonorrhoeae	MMX 7002	Micromyx, LLC
N. gonorrhoeae	MMX 7005	Micromyx, LLC
Escherichia coli	KLE700	(*48*)
Escherichia coli	KLE701 *tolC::tet*	(*48*)
Klebsiella pneumoniae	ATCC 13883	ATCC
Acinetobacter baumannii	ATCC 19606	ATCC
Pseudomonas aeruginosa	ATCC 27853	ATCC
Moraxella catarrhalis	ATCC 8716	ATCC
Legionella pneumophila	ATCC 33153	ATCC
Haemophilus influenzae	ATCC 35056	ATCC

Staphylococcus aureus	BAA-1717		ATCC
Staphylococcus aureus	MRSA-1234547263		(*49*)
Staphylococcus aureus	MRSA-1094		(*50*)
Staphylococcus aureus	ATCC 35556		ATCC
Staphylococcus aureus	NRS-77		BEI Resources
Staphylococcus aureus	MSSA		(*50*)
Staphylococcus aureus	N315, NRS-70		BEI Resources
Staphylococcus aureus	ATCC 25923		ATCC
Staphylococcus aureus	THC1516		(*51*)
Streptococcus pneumoniae	ATCC 49619		ATCC
Mycoplasma pneumoniae	ATCC 15531		ATCC
plasmid name	description		source
pET28-H10arfArnc	plasmid to produce non-stop ribosomes *in vivo*		this work
pNL3.1	nano-luciferase encoding plasmid		Promega
pMC1	Nano-luciferase gene cloned into the NcoI and BamH1 sites of pET28		this work
DNA name	description	sequence	source
T7 universal	primer	TAATACGACTCACTATAGGG	ThermoFisher
nanoluc-ns	primer	CCCCCCGGTTACCCGGAAGAGCAGGGAGCCGTC	this work
nanoluc-stop	primer	TTACAGAATCTCCTCGAACAGCCG	this work
tmRNA-nl template	synthetic DNA cassette	GGGGCTGATTCTGGATTCGACGGGATTTGCGAAACCCAAGGTGCATGCCGAGGGGCGGTTGGCCTCGTAAAAAGCCGCAAAAAATAGTCGCAGTCTCCGGATGGCGCCTTTTTAAAAAAATTTCTTAATAACAATTTTTTTAGCCCTCTCTCCCTAGCCTCCGCTCTTAGGACGGGGATCAAGAGAGGTCAAACCCAAAAGAGATCGCGTGGAAGCCCTGCCTGGGGTTGAAGCGTTAAAACTTAATCAGGCTAGTTTGTTAGTGGCGTGTCCGTCCGCAGCTGGCAAGCGAATGTAAAGACTGACTAAGCATGTAGTACCGAGGATGTAGGAATTTCGGACGCGGGTTCAACTCCCGCCAGCTCCACCA	this work

858

859

860 **SUPPLEMENTAL FIGURES**

A.

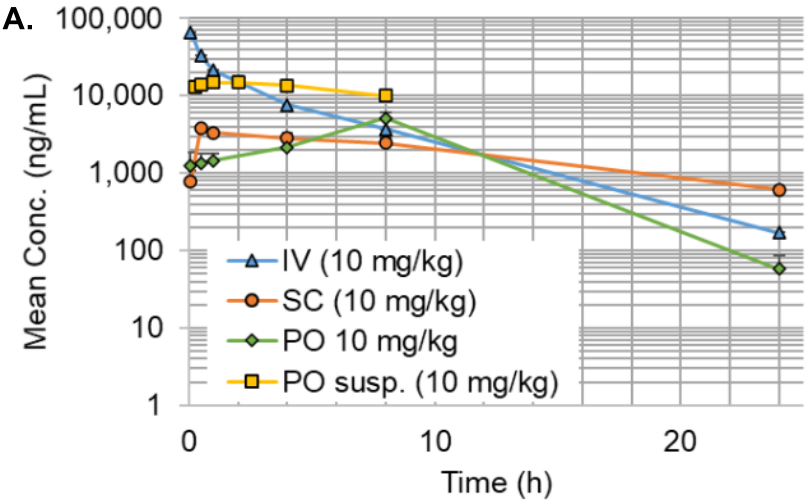

B.

	$T_{1/2}$ (hr)	$C_{0/max}$ (ng/mL)	AUC_{last} (hr*ng/mL)	V_{ss} (mL/kg)	Cl (mL/hr/kg)	%F (Last)
10 mg/kg IV	3.55	76,507	137,462	266	72.6	-
10 mg/kg SC	8.76	3,793	46,916	-	-	34
25 mg/kg SC	-	5,100	76,085	-	-	-
10 mg/kg PO	-	5,110	62,617	-	-	46
10 mg/kg susp. PO	-	14,812	181,695	-	-	>95*

861

862

863 **Supplemental Figure S1. Pharmacokinetic properties of MXB-4132** (A) Graphical
864 presentation of murine plasma concentration over time for MBX-4132. For clarity, error bars are
865 only shown in the positive direction. "susp." Refers to the suspension formulation studies
866 performed at Neosome, all other data is from liquid formulation performed at Charles River Labs.
867 (B) Calculated parameters for each dosing regimen of MBX-4132. %F for the 10 mg/kg PO
868 suspension formulation is an estimate based on the IV data for different mouse species and
869 gender.

870

871

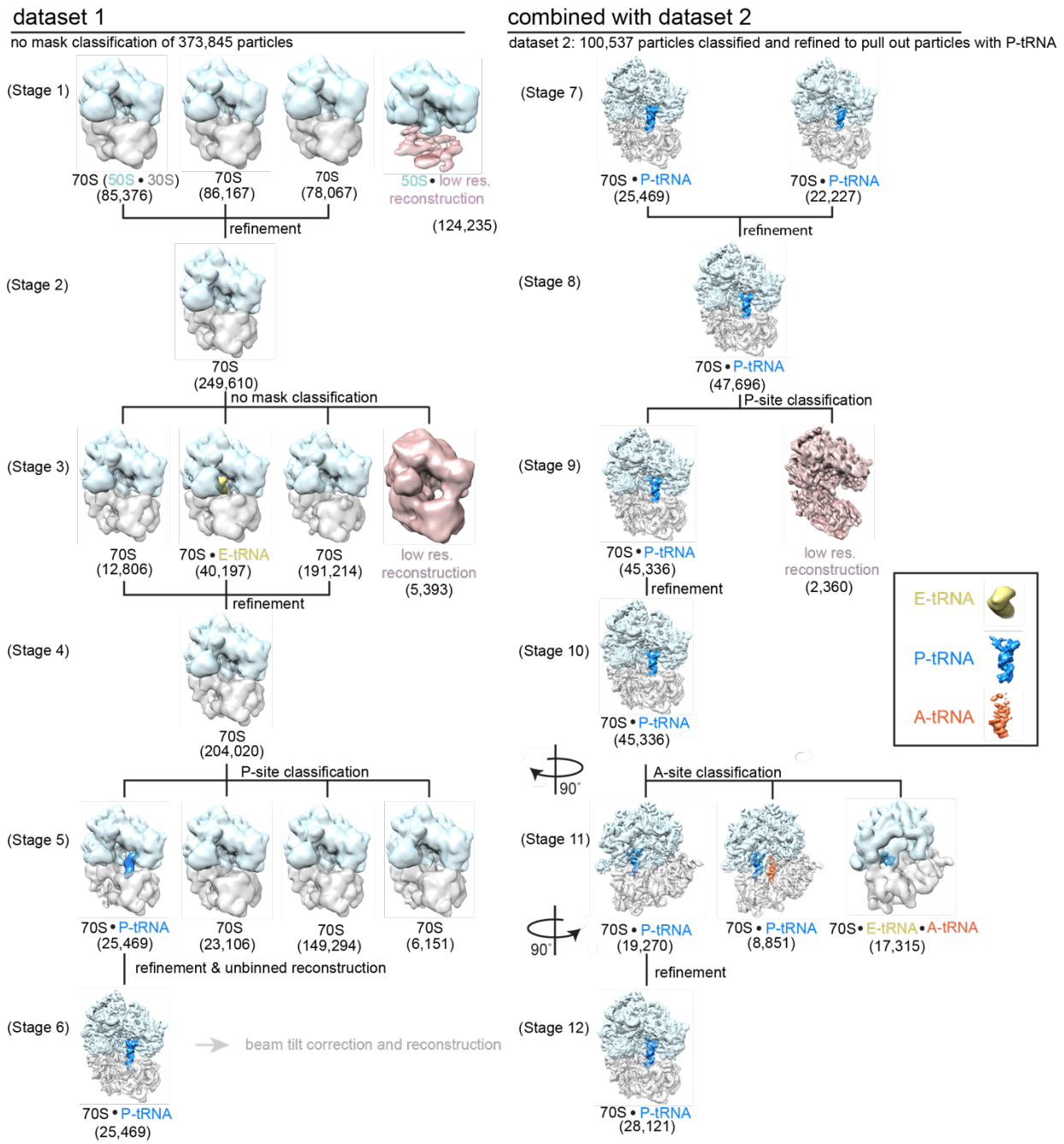

Supplemental Figure S2. Classification of cryo-EM datasets of *E. coli* 70S complex containing P-site tRNA and KKL-2098. To extract 70S particles with P-site tRNA and the KKL-2098 molecule several classification and refinement steps were performed. Stage 1) All particles were refined and reconstructed, then classification without alignment was performed to split the particles into 4 classes. Stage 2) 50S particles from stage 1 (shown in blue) were removed and the remaining particles refined. Stage 3) The aligned particles from stage 2 were classified into 4 classes. Stage 4) Particles contributing to the low-resolution reconstruction (pink) and 70S structures containing E-site tRNA (yellow) were removed and the remaining particles refined. Stage 5) Particles were classified without alignment into 4 classes using a P-site mask to identify particles with P-tRNA (blue). Stage 6) Particles containing P-tRNA were combined,

unbinned and refined. Stage 7) Particles were beam-tilt corrected. Stage 8) Particles from both datasets were combined and refined together. Stage 9) The combined particles were classified using a P-site mask. Stage 10) Particles contributing to the lower-resolution reconstruction were eliminated and 70S/P-tRNA particles were refined. Stage 11) The reconstruction from stage 10 contained some A-site tRNA density, so a focused classification without alignment using an A-site mask was performed. Ribosomes are shown at 90° rotated view in respect to stage 10. Stage 12) 70S particles containing A-site tRNA (orange) were eliminated and 70S/P-tRNA particles were refined to an overall resolution of 3.2 Å. The numbers of particles that make up each reconstruction are depicted for each complex.

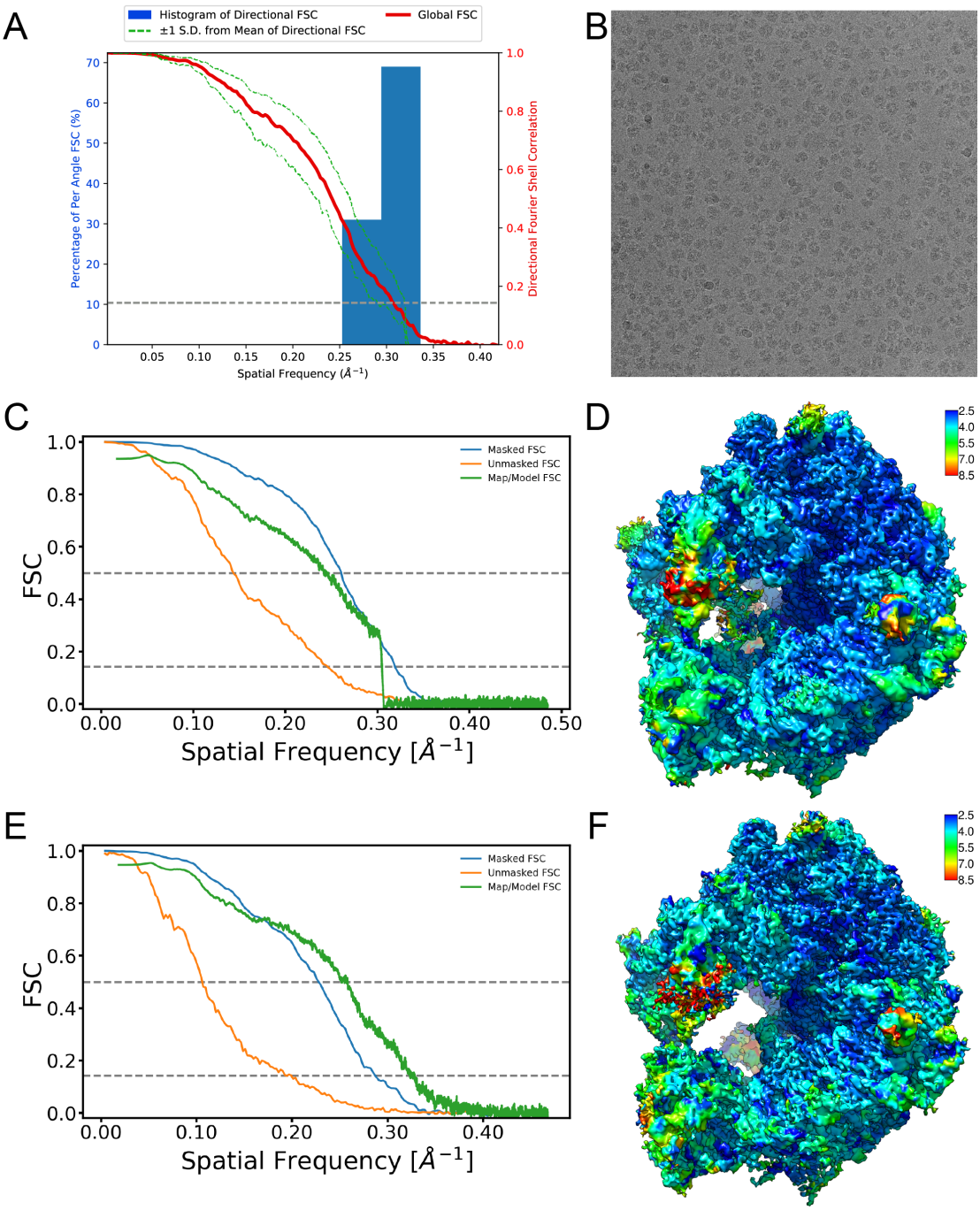

Supplemental Figure S3. Resolution characterization and quality of cryo-EM maps. (A) 3D FSC plot (*14*) showing degree of directional anisotropy for the 70S•P-tRNA•KKL map. (B) A representative micrograph from the cryo-EM dataset. (C) FSC plots for the 70S•P-tRNA•KKL map for the independent half maps (orange) masked (cyan), and map/model FSC (green). Dotted lines are shown at $FSC_{0.5}$ and $FSC_{0.143}$. (D) Local resolution estimate for the 70S-P-tRNA-KKL-2098 map estimated from blocres (*15*) . The map is colored from highest resolution (blue) to lowest resolution (red). (E) FSC plots for the 70S-KKL-2098 map for the independent half maps (orange) masked (cyan), and map/model FSC (green). (F) Local resolution estimate for the 70S•KKL map colored as in D.

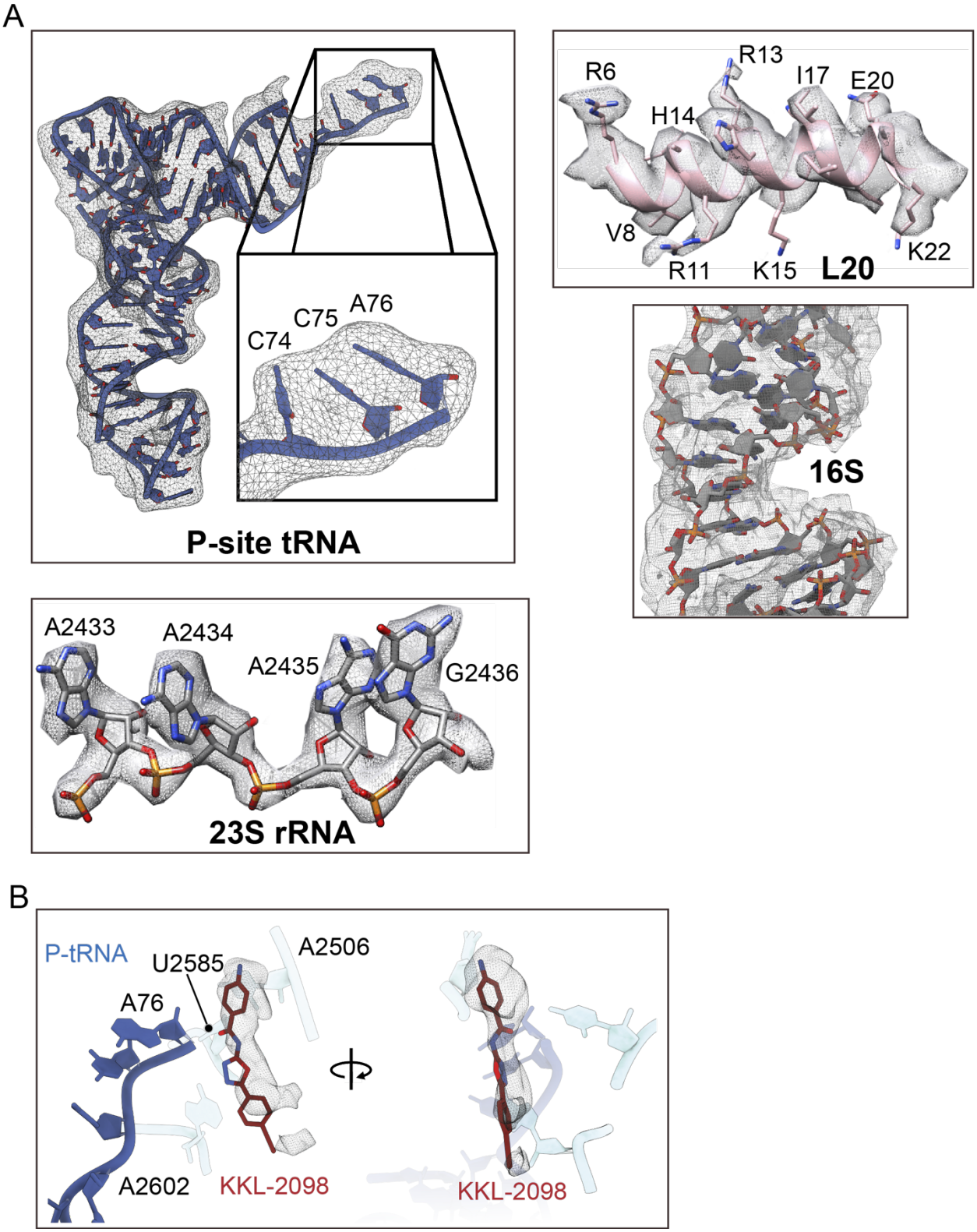

Supplemental Figure S4. Data quality of representative areas of the 70S-P-tRNA-KKL-2098 map. (A) Representative map quality of the P-site tRNA with the inset showing the CCA end. Map quality for ribosomal protein L20, 16S rRNA and 23S rRNA. (B) Map quality of KKL-2098.

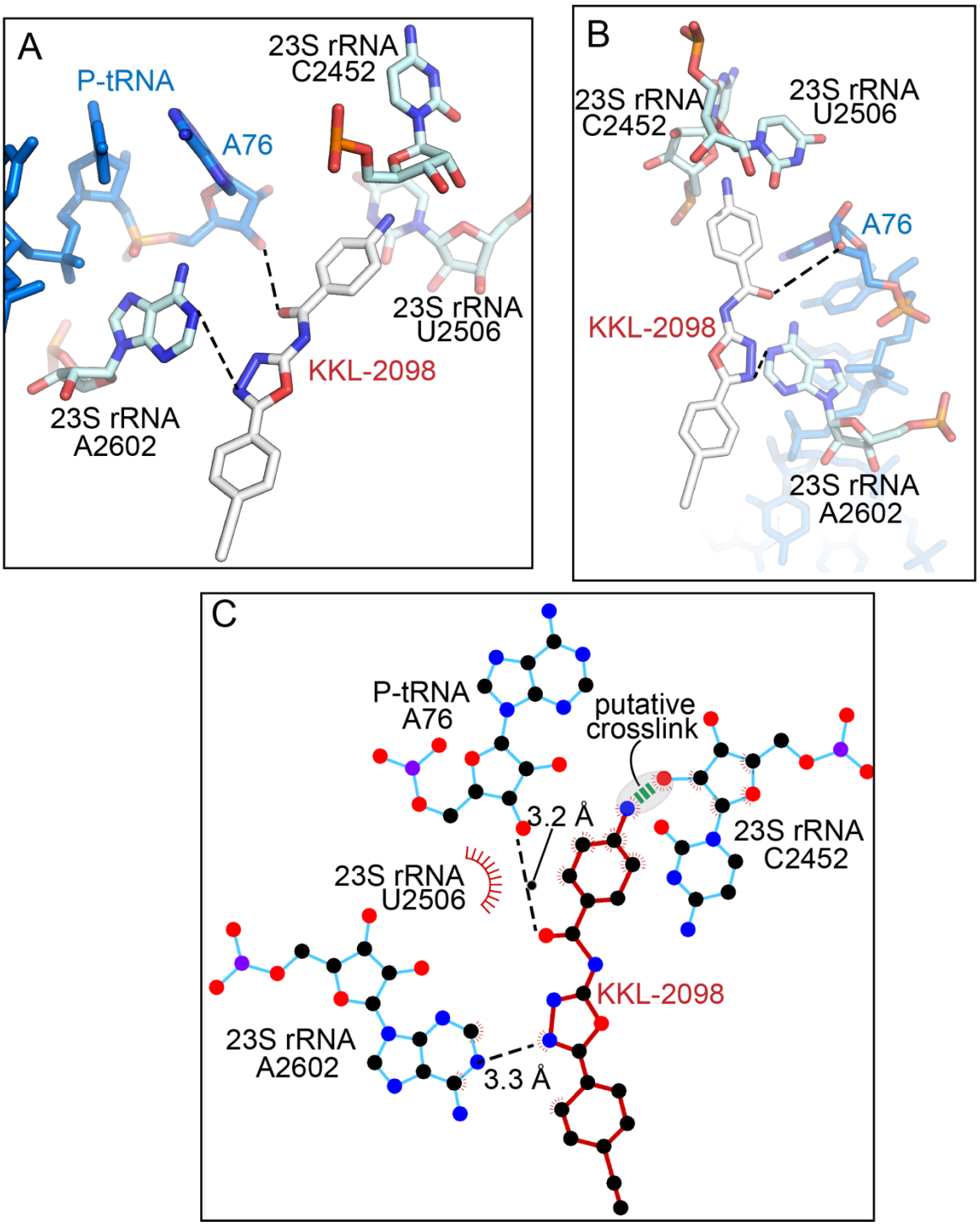

Supplemental Figure S5. Interaction network of KKL-2098 with the ribosome. (A) Interactions with of KKL-2098 with P-site tRNA A76 and 23 rRNA nucleotides C2452, A2506, and A2602 with a ~90º rotation in panel B. (C) A 2-dimensional representation of these interactions using LigPlot+ (*52*).

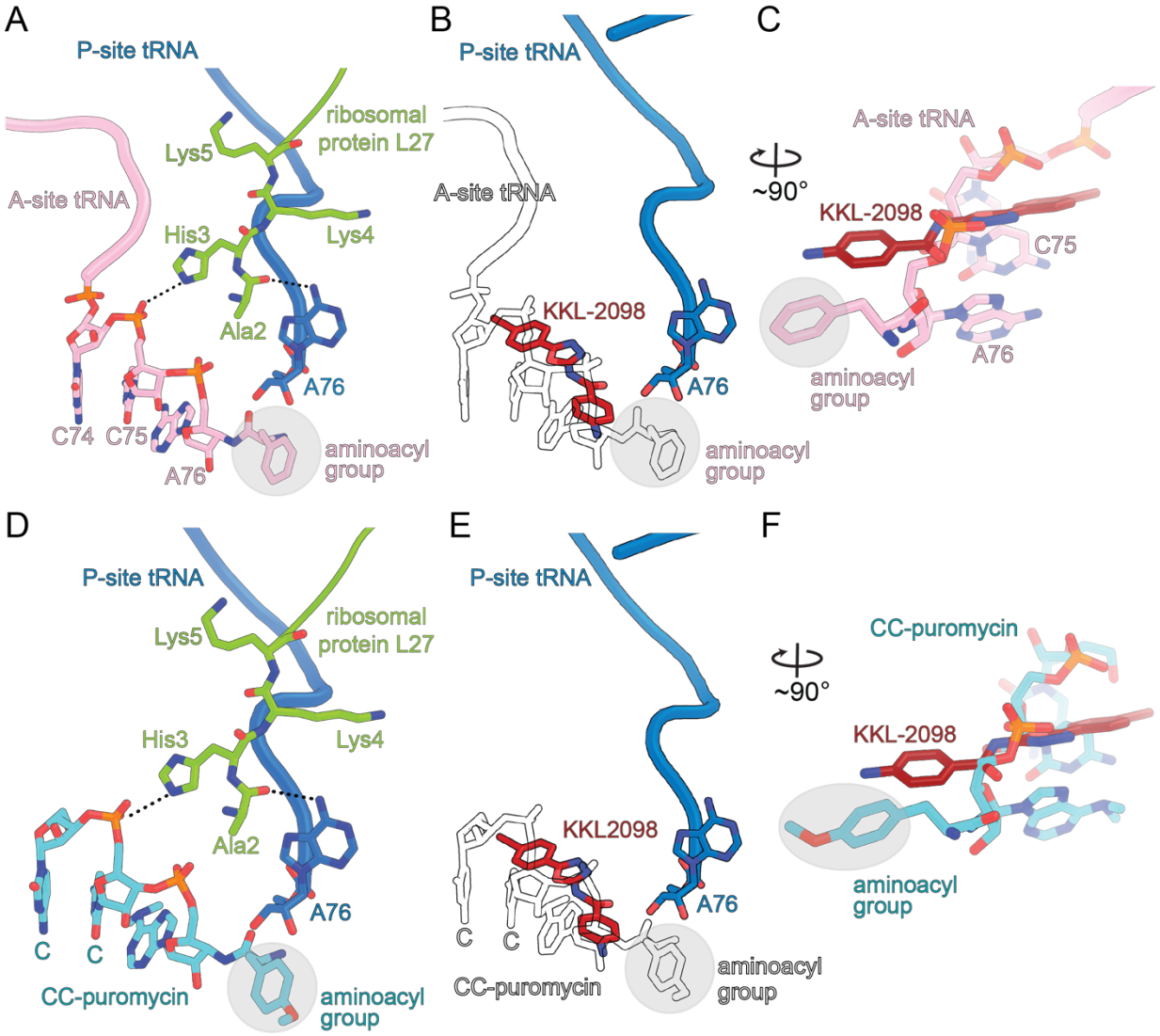

Supplemental Figure S6. Comparison of KKL-2098 to A-site tRNA and CC-puromycin locations. (A) The N terminus of L27 is stabilized when an aminoacylated (aa)-tRNA is bound at the A site (PDB ID 4V5C). (B) Overlay of aa-tRNA and KKL-2098. (C) A ~90º rotation of panel B shows how KKL-2098 overlaps primarily with the phosphate of A76. (D) The stabilization of the N terminus of L27 also occurs when CC-puromycin is bound (PDB ID 6OTR). (E) Overlay of CC-puromycin and KKL-2098. (F) A ~90º rotation of panel B shows how KKL-2098 overlaps primarily with the phosphate of CC-puromycin.

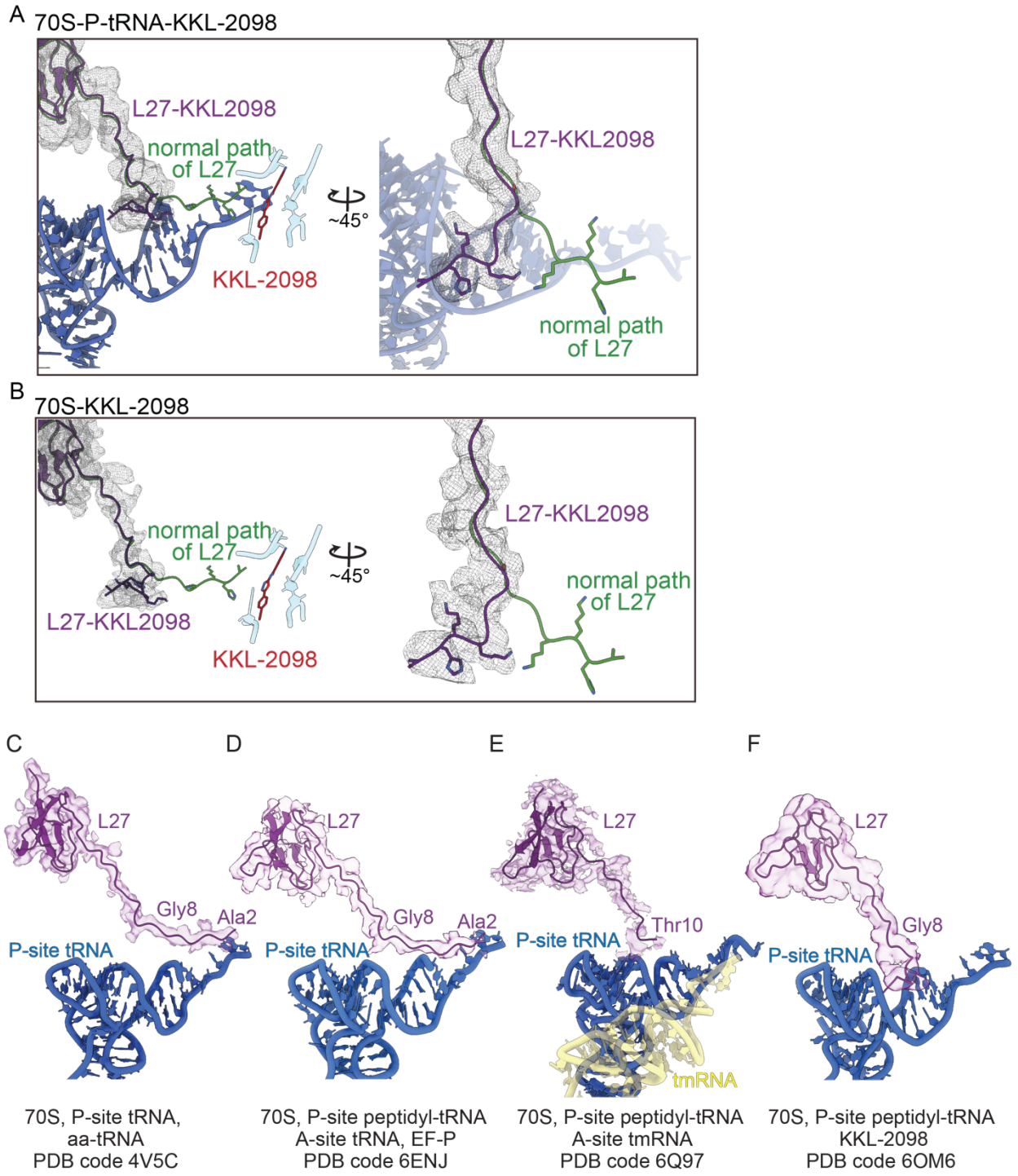

Supplemental Figure S7. L27 map quality and its location in other structures. (A) In the 70S-P-site tRNA-KKL-2098 structure, the N terminus of L27 (purple) moves ~180º away from the PTC. The previously observed position of L27 is shown in green (PDB ID 6ENU). (B) In the 70S-KKL-2098 structure, L27 adopts a similar position as when P-site tRNA-KKL-2098 is bound as shown in panel A. It is proposed that these particles represent a complex where peptidyl-P-site tRNA has dropped off during preparation. Position and electron potential maps of L27 in PDB code 4V5C (C), 6ENJ (D), 6Q97 (E) and 6OM6 (F).

Supplemental References

1. J. Boström, A. Hogner, A. Llinàs, E. Wellner, A. T. Plowright, Oxadiazoles in Medicinal Chemistry. *J. Med. Chem.* **55**, 1817–1830 (2012).

2. S. T. Nguyen, S. M. Kwasny, X. Ding, S. C. Cardinale, C. T. McCarthy, H.-S. Kim, H. Nikaido, N. P. Peet, J. D. Williams, T. L. Bowlin, T. J. Opperman, Structure-activity relationships of a novel pyranopyridine series of Gram-negative bacterial efflux pump inhibitors. *Bioorg. Med. Chem.* **23**, 2024–2034 (2015).

3. J. Kaur, M. Soto-Velasquez, Z. Ding, A. Ghanbarpour, M. A. Lill, R. M. van Rijn, V. J. Watts, D. P. Flaherty, Optimization of a 1,3,4-oxadiazole series for inhibition of Ca2+/calmodulin-stimulated activity of adenylyl cyclases 1 and 8 for the treatment of chronic pain. *Eur. J. Med. Chem.* **162**, 568–585 (2019).

4. S.-J. Yang, J.-H. Choe, A. Abdildinova, Y.-D. Gong, A Highly Efficient Diversification of 2-Amino/Amido-1,3,4-oxadiazole and 1,3,4-Thiadiazole Derivatives via Reagent-Based Cyclization of Thiosemicarbazide Intermediate on Solid-Phase. *ACS Comb. Sci.* **17**, 732–741 (2015).

5. M. Sakamoto, K. Miyazawa, Y. Tomimatsu, Addition Reactions of Heterocumulenes. II. 1, 4-Cycloaddition Reactions of Diphenylketene with Azadienes. *Chem. Pharm. Bull. (Tokyo)*. **24**, 2532–2540 (1976).

6. Clinical and Laboratory Standards Institute, Ed., *Methods for dilution antimicrobial susceptibility tests for bacteria that grow aerobically: M07-A10 ; approved standard* (Committee for Clinical Laboratory Standards, Wayne, PA, 10. ed., 2015), *Documents / Clinical and Laboratory Standards Institute*.

7. D. E. Macfarlane, T. F. Elias-Jones, Improved media for the culture of Neisseria gonorrhoeae. *J. Med. Microbiol.* **13**, 597–607 (1980).

8. M. M. Butler, S. L. Waidyarachchi, K. L. Connolly, A. E. Jerse, W. Chai, R. E. Lee, S. A. Kohlhoff, D. L. Shinabarger, T. L. Bowlin, Aminomethyl Spectinomycins as Therapeutics for Drug-Resistant Gonorrhea and Chlamydia Coinfections. *Antimicrob. Agents Chemother.* **62** (2018), doi:10.1128/AAC.00325-18.

9. M. Ohnishi, D. Golparian, K. Shimuta, T. Saika, S. Hoshina, K. Iwasaku, S. Nakayama, J. Kitawaki, M. Unemo, Is Neisseria gonorrhoeae Initiating a Future Era of Untreatable Gonorrhea?: Detailed Characterization of the First Strain with High-Level Resistance to Ceftriaxone. *Antimicrob. Agents Chemother.* **55**, 3538–3545 (2011).

10. M. Ohnishi, T. Saika, S. Hoshina, K. Iwasaku, S. Nakayama, H. Watanabe, J. Kitawaki, Ceftriaxone-Resistant Neisseria gonorrhoeae, Japan. *Emerg. Infect. Dis.* **17**, 148–149 (2011).

11. Pillai SK, Moellering RC, Eliopoulos GM, in *Antibiotics in Laboratory Medicine, 5th ed.* (Lippincott Williams & Wilkins, Philadelphia, PA., 2005), pp. 365–440.

12. A. S. Dixon, M. K. Schwinn, M. P. Hall, K. Zimmerman, P. Otto, T. H. Lubben, B. L. Butler, B. F. Binkowski, T. Machleidt, T. A. Kirkland, M. G. Wood, C. T. Eggers, L. P. Encell, K. V. Wood, NanoLuc

982 Complementation Reporter Optimized for Accurate Measurement of Protein Interactions in Cells.
983 *ACS Chem. Biol.* **11**, 400–408 (2016).

984 13. T.-W. Kim, J.-W. Keum, I.-S. Oh, C.-Y. Choi, C.-G. Park, D.-M. Kim, Simple procedures for the
985 construction of a robust and cost-effective cell-free protein synthesis system. *J. Biotechnol.* **126**,
986 554–561 (2006).

987 14. N. S. Ramadoss, J. N. Alumasa, L. Cheng, Y. Wang, S. Li, B. S. Chambers, H. Chang, A. K. Chatterjee,
988 A. Brinker, I. H. Engels, K. C. Keiler, Small molecule inhibitors of trans-translation have broad-
989 spectrum antibiotic activity. *Proc. Natl. Acad. Sci. U. S. A.* **110**, 10282–10287 (2013).

990 15. C. J. Woolstenhulme, S. Parajuli, D. W. Healey, D. P. Valverde, E. N. Petersen, A. L. Starosta, N. R.
991 Guydosh, W. E. Johnson, D. N. Wilson, A. R. Buskirk, Nascent peptides that block protein synthesis
992 in bacteria. *Proc. Natl. Acad. Sci.* **110**, E878–E887 (2013).

993 16. Clinical and Laboratory Standards Institute, *Performance standards for antimicrobial susceptibility*
994 *testing* (2017).

995 17. N. J. Marshall, C. J. Goodwin, S. J. Holt, A critical assessment of the use of microculture tetrazolium
996 assays to measure cell growth and function. *Growth Regul.* **5**, 69–84 (1995).

997 18. W. Kuhnz, H. Gieschen, Predicting the oral bioavailability of 19-nortestosterone progestins in vivo
998 from their metabolic stability in human liver microsomal preparations in vitro. *Drug Metab. Dispos.*
999 *Biol. Fate Chem.* **26**, 1120–1127 (1998).

1000 19. R. S. Obach, J. G. Baxter, T. E. Liston, B. M. Silber, B. C. Jones, F. MacIntyre, D. J. Rance, P. Wastall,
1001 The prediction of human pharmacokinetic parameters from preclinical and in vitro metabolism
1002 data. *J. Pharmacol. Exp. Ther.* **283**, 46–58 (1997).

1003 20. I. J. Hidalgo, T. J. Raub, R. T. Borchardt, Characterization of the human colon carcinoma cell line
1004 (Caco-2) as a model system for intestinal epithelial permeability. *Gastroenterology*. **96**, 736–749
1005 (1989).

1006 21. M. J. Banker, T. H. Clark, J. A. Williams, Development and validation of a 96-well equilibrium
1007 dialysis apparatus for measuring plasma protein binding. *J. Pharm. Sci.* **92**, 967–974 (2003).

1008 22. C. D. Bevan, R. S. Lloyd, A high-throughput screening method for the determination of aqueous
1009 drug solubility using laser nephelometry in microtiter plates. *Anal. Chem.* **72**, 1781–1787 (2000).

1010 23. B. N. Ames, J. Mccann, E. Yamasaki, Methods for detecting carcinogens and mutagens with the
1011 Salmonella/mammalian-microsome mutagenicity test. *Mutat. Res.* **31**, 347–364 (1975).

1012 24. D. M. Maron, B. N. Ames, Revised methods for the Salmonella mutagenicity test. *Mutat. Res.* **113**,
1013 173–215 (1983).

1014 25. K. Mortelmans, E. Zeiger, The Ames Salmonella/microsome mutagenicity assay. *Mutat. Res.* **455**,
1015 29–60 (2000).

1016 26. V. C. Abraham, D. L. Towne, J. F. Waring, U. Warrior, D. J. Burns, Application of a high-content
1017 multiparameter cytotoxicity assay to prioritize compounds based on toxicity potential in humans.
1018 *J. Biomol. Screen.* **13**, 527–537 (2008).

1019 27. L. D. Marroquin, J. Hynes, J. A. Dykens, J. D. Jamieson, Y. Will, Circumventing the Crabtree effect:
1020 replacing media glucose with galactose increases susceptibility of HepG2 cells to mitochondrial
1021 toxicants. *Toxicol. Sci. Off. J. Soc. Toxicol.* **97**, 539–547 (2007).

1022 28. D. G. Gibson, L. Young, R.-Y. Chuang, J. C. Venter, C. A. Hutchison, H. O. Smith, Enzymatic assembly
1023 of DNA molecules up to several hundred kilobases. *Nat. Methods*. **6**, 343–345 (2009).

1024 29. Y. Chadani, E. Matsumoto, H. Aso, T. Wada, K. Kutsukake, S. Sutou, T. Abo, *trans*-translation-
1025 mediated tight regulation of the expression of the alternative ribosome-rescue factor ArfA in
1026 *Escherichia coli*. *Genes Genet. Syst.* **86**, 151–163 (2011).

1027 30. F. Garza-Sánchez, R. E. Schaub, B. D. Janssen, C. S. Hayes, tmRNA regulates synthesis of the ArfA
1028 ribosome rescue factor. *Mol. Microbiol.* **80**, 1204–1219 (2011).

1029 31. Y. Zhang, S. Hong, A. Ruangprasert, G. Skiniotis, C. M. Dunham, Alternative mode of E-site tRNA
1030 binding in the presence of a downstream mRNA stem-loop at the entrance channel. *Struct. Lond.*
1031 *Engl. 1993*. **26**, 437-445.e3 (2018).

1032 32. J. N. Alumasa, P. S. Manzanillo, N. D. Peterson, T. Lundrigan, A. D. Baughn, J. S. Cox, K. C. Keiler,
1033 Ribosome Rescue Inhibitors Kill Actively Growing and Nonreplicating Persister Mycobacterium
1034 tuberculosis Cells. *ACS Infect. Dis.* **3**, 634–644 (2017).

1035 33. J. H. Mendez, A. Mehrani, P. Randolph, S. Stagg, Throughput and resolution with a next-generation
1036 direct electron detector. *IUCrJ*. **6**, 1007–1013 (2019).

1037 34. C. Suloway, J. Pulokas, D. Fellmann, A. Cheng, F. Guerra, J. Quispe, S. Stagg, C. S. Potter, B.
1038 Carragher, Automated molecular microscopy: the new Leginon system. *J. Struct. Biol.* **151**, 41–60
1039 (2005).

1040 35. G. C. Lander, S. M. Stagg, N. R. Voss, A. Cheng, D. Fellmann, J. Pulokas, C. Yoshioka, C. Irving, A.
1041 Mulder, P.-W. Lau, D. Lyumkis, C. S. Potter, B. Carragher, Appion: an integrated, database-driven
1042 pipeline to facilitate EM image processing. *J. Struct. Biol.* **166**, 95–102 (2009).

1043 36. K. Zhang, Gctf: Real-time CTF determination and correction. *J. Struct. Biol.* **193**, 1–12 (2016).

1044 37. A. Rohou, N. Grigorieff, CTFFIND4: Fast and accurate defocus estimation from electron
1045 micrographs. *J. Struct. Biol.* **192**, 216–221 (2015).

1046 38. L. K. Sheth, A. L. Piotrowski, N. R. Voss, Visualization and quality assessment of the contrast
1047 transfer function estimation. *J. Struct. Biol.* **192**, 222–234 (2015).

1048 39. N. R. Voss, C. K. Yoshioka, M. Radermacher, C. S. Potter, B. Carragher, DoG Picker and TiltPicker:
1049 software tools to facilitate particle selection in single particle electron microscopy. *J. Struct. Biol.*
1050 **166**, 205–213 (2009).

1051 40. A. M. Roseman, FindEM--a fast, efficient program for automatic selection of particles from
1052 electron micrographs. *J. Struct. Biol.* **145**, 91–99 (2004).

1053 41. S. H. W. Scheres, RELION: implementation of a Bayesian approach to cryo-EM structure
1054 determination. *J. Struct. Biol.* **180**, 519–530 (2012).

1055 42. A. Korostelev, S. Trakhanov, M. Laurberg, H. F. Noller, Crystal structure of a 70S ribosome-tRNA
1056 complex reveals functional interactions and rearrangements. *Cell*. **126**, 1065–1077 (2006).

1057 43. R. M. Voorhees, A. Weixlbaumer, D. Loakes, A. C. Kelley, V. Ramakrishnan, Insights into substrate
1058 stabilization from snapshots of the peptidyl transferase center of the intact 70S ribosome. *Nat.*
1059 *Struct. Mol. Biol.* **16**, 528–533 (2009).

1060 44. P. D. Adams, P. V. Afonine, G. Bunkóczi, V. B. Chen, I. W. Davis, N. Echols, J. J. Headd, L.-W. Hung,
1061 G. J. Kapral, R. W. Grosse-Kunstleve, A. J. McCoy, N. W. Moriarty, R. Oeffner, R. J. Read, D. C.
1062 Richardson, J. S. Richardson, T. C. Terwilliger, P. H. Zwart, PHENIX: a comprehensive Python-based
1063 system for macromolecular structure solution. *Acta Crystallogr. D Biol. Crystallogr.* **66**, 213–221
1064 (2010).

1065 45. Y. Z. Tan, P. R. Baldwin, J. H. Davis, J. R. Williamson, C. S. Potter, B. Carragher, D. Lyumkis,
1066 Addressing preferred specimen orientation in single-particle cryo-EM through tilting. *Nat.*
1067 *Methods*. **14**, 793–796 (2017).

1068 46. J. B. Heymann, Guidelines for using Bsoft for high resolution reconstruction and validation of
1069 biomolecular structures from electron micrographs. *Protein Sci. Publ. Protein Soc.* **27**, 159–171
1070 (2018).

1071 47. B. A. Maguire, A. D. Beniaminov, H. Ramu, A. S. Mankin, R. A. Zimmermann, A Protein Component
1072 at the Heart of an RNA Machine: The Importance of Protein L27 for the Function of the Bacterial
1073 Ribosome. *Mol. Cell*. **20**, 427–435 (2005).

1074 48. G. Tegos, F. R. Stermitz, O. Lomovskaya, K. Lewis, Multidrug pump inhibitors uncover remarkable
1075 activity of plant antimicrobials. *Antimicrob. Agents Chemother.* **46**, 3133–3141 (2002).

1076 49. D. Aiello, M. H. Barnes, E. E. Biswas, S. B. Biswas, S. Gu, J. D. Williams, T. L. Bowlin, D. T. Moir,
1077 Discovery, characterization and comparison of inhibitors of Bacillus anthracis and Staphylococcus
1078 aureus replicative DNA helicases. *Bioorg. Med. Chem.* **17**, 4466–4476 (2009).

1079 50. T. J. Opperman, S. M. Kwasny, J. D. Williams, A. R. Khan, N. P. Peet, D. T. Moir, T. L. Bowlin, Aryl
1080 rhodanines specifically inhibit staphylococcal and enterococcal biofilm formation. *Antimicrob.*
1081 *Agents Chemother.* **53**, 4357–4367 (2009).

1082 51. B. E. Gonzalez, G. Martinez-Aguilar, K. G. Hulten, W. A. Hammerman, J. Coss-Bu, A. Avalos-
1083 Mishaan, E. O. Mason, S. L. Kaplan, Severe Staphylococcal sepsis in adolescents in the era of
1084 community-acquired methicillin-resistant Staphylococcus aureus. *Pediatrics*. **115**, 642–648 (2005).

1085 52. R. A. Laskowski, M. B. Swindells, LigPlot+: multiple ligand-protein interaction diagrams for drug
1086 discovery. *J. Chem. Inf. Model.* **51**, 2778–2786 (2011).

1087